HELLENIC REPUBLIC
National and Kapodistrian University of Athens
EST. 1837

"ALEXANDER FLEMING"
Biomedical Sciences Research Center

NATIONAL AND KAPODISTRIAN UNIVERSITY OF ATHENS

FACULTY OF MEDICINE

MEDICAL SCHOOL

MASTER'S PROGRAM in BASIC MEDICAL SCIENCES
"MOLECULAR BIOMEDICINE: MECHANISMS OF DISEASE, MOLECULAR AND CELLULAR THERAPIES, AND BIOINNOVATION"

MASTER'S THESIS

Setup and optimization of phosphoproteomic methodologies for the analysis of tissues from DUSP8 CRISPR-knockout mice

ALEXANDROS ZOGRAFAKIS
Biologist, BSc

Supervisor: Dr. GEORGE PANAYOTOU
Researcher A
BSRC "Alexander Fleming"

ATHENS

SEPTEMBER 2018

EXAMINATION COMMITTEE:

1) Dr. George Panayotou, Researcher A', Division of Molecular Oncology, BSRC "Alexander Fleming"

2) Dr. Vassiliki Kostourou, Researcher B', Division of Immunology, BSRC "Alexander Fleming"

3) Prof. Michael Koutsilieris, Professor of Experimental Physiology, Medical School, National and Kapodistrian University of Athens

Abstract

The Mitogen Activated Protein Kinase (MAPK) pathway is involved in many different biological processes, including cell proliferation, differentiation, survival, apoptosis and inflammation and is associated with a variety of pathological diseases, like cancer and neurodegeneration. It consists of a three-level cascade of phosphorylation events which either lead to the activation of a nuclear transcription factor for gene expression regulation or the activation of a cytoplasmic protein. The MAPK pathway includes three major subfamilies: the extracellular-signal regulated kinase (ERK1/2), the p38 kinase and the c-Jun N-terminal kinase (JNK) subfamilies. Even though each pathway is involved in different biological processes, events of co-activation and co-regulation are quite frequent, especially in the case of JNK/p38 kinases, which are also called stress-activated protein kinases (SAPKs). MAP kinase activity is regulated by a specific group of phosphatases called mitogen activated protein kinase phosphatases (MKPs). MKPs belong to a larger group called dual specificity phosphatases (DUSPs). This three-part project focuses on DUSP8, a JNK/p38 specific phosphatase, and its inhibition by arsenite, a JNK pathway-enhancing and oxidative stress inducing agent. The first part concerned the optimization of a phosphoproteomics workflow from cell culture to data analysis. Immunoblotting with specific antibodies of lysates from differentially starved and stimulated HEK293T cells provided information about the arsenite stimulation conditions, where a clear effect of phosphorylation was observed. Arsenite was found to be effective in the overall stimulation of phosphorylation. The following steps were to determine the mass spectrometry (MS) parameters and the sample preparation method with the highest protein and peptide yield after phosphopeptide enrichment and nanoLC-MS/MS analysis. Three methods were examined: Filter-aided sample preparation (FASP), solid-phase-enhanced sample preparation (SP3) and Trifluoroethanol-based digestion (TFE). Determined stimulation periods, MS parameters and sample preparation methods were then implemented in the second part of the project, which involved the phosphoproteome LC-MS/MS analysis of primary mouse embryonic fibroblasts derived from DUSP8-KO mice generated by CRISPR technology, and their WT littermates. Increased phosphorylation on a large number of proteins was detected in DUSP8-KO MEFs. Almost no phosphotyrosine residues were detected, possibly due to their transient nature. Also, increased

phosphorylation of ERK2 substrates in DUSP8-KO MEFs suggested a possible regulation of ERK2 activity by DUSP8. In the last part, a comparative whole proteome analysis was conducted in tissues of DUSP8-KO mice and their WT littermates. The results suggested that overactivation of the JNK pathway due to DUSP8 deficiency in the brain leads to mitochondrial apoptosis and neurodegeneration. Additionally, the ERK1/2-driven response to oxidative stress in the brain of DUSP8-KO mice is possibly mediated by increased expression of B-Raf, one of the identified proteins in the comparative whole proteome analysis.

Περίληψη

Το μονοπάτι των πρωτεϊνικών κινασών που ενεργοποιούνται από μιτογόνα (MAPKs) συμμετέχει σε πολλές διαφορετικές βιολογικές διεργασίες, όπως ο κυτταρικός πολλαπλασιασμός, η κυτταρική διαφοροποίηση, επιβίωση, απόπτωση και φλεγμονή. Σχετίζεται και με μια πληθώρα ασθενειών, όπως ο καρκίνος και ο νευροεκφυλισμός. Αποτελείται από μία αλληλουχία αντιδράσεων φωσφορυλίωσης που χωρίζεται σε τρία επίπεδα και οδηγεί είτε στην ενεργοποίηση ενός πυρηνικού μεταγραφικού παράγοντα για τη ρύθμιση της έκφρασης γονιδίων είτε στην ενεργοποίηση κάποιας κυτταροπλασματικής πρωτεΐνης. Περιλαμβάνει τρεις μεγάλες υποοικογένειες: Τις ERK1/2 κινάσες, τις p38 κινάσες και τις c-Jun N-terminal κινάσες (JNK). Ακόμη κι αν κάθε επιμέρους μονοπάτι συμμετέχει γενικά σε διαφορετικές διεργασίες, υπάρχουν συχνά φαινόμενα όπου παρατηρείται συνενεργοποίηση και συρρύθμιση, ειδικά στην περίπτωση των JNK/p38 κινασών, που είναι γνωστές και σαν κινάσες που ενεργοποιούνται από το στρες (SAPKs). Η δράση των MAPKs ρυθμίζεται από μία συγκεκριμένη ομάδα φωσφατασών, τις φωσφατάσες των πρωτεϊνικών κινασών που ενεργοποιούνται από μιτογόνα (MKPs). Οι MKPs ανήκουν σε μία μεγαλύτερη ομάδα πρωτεϊνών, τις φωσφατάσες διπλής ειδικότητας (DUSPs). Η διατριβή αυτή επικεντρώνεται στην DUSP8, μια φωσφατάση ειδική για JNK/p38 κινάσες, και στην αναστολή της από το αρσενικό, έναν παράγοντα που προκαλεί οξειδωτικό στρες και ενισχύει το μονοπάτι των JNK κινασών. Το πρώτο μέρος της διατριβής αφορά τη βελτιστοποίηση ενός πρωτοκόλλου φωσφοπρωτεομικής, από το βήμα της κυτταρικής καλλιέργειας ως το βήμα της ανάλυσης δεδομένων. Η ανάλυση με western χρησιμοποιώντας συγκεκριμένα αντισώματα σε λύματα HEK293T κυττάρων που είχαν καλλιεργηθεί σε διαφορετικές περιόδους στρεσογόνας διέγερσης, παρείχαν πληροφορίες σχετικά με τις περιόδους διέγερσης με αρσενικό όπου παρατηρήθηκαν σαφείς επιδράσεις στα γενικά επίπεδα φωσφορυλίωσης. Το αρσενικό φάνηκε να διεγείρει αποτελεσματικά την αύξηση των γενικών επιπέδων φωσφορυλίωσης. Τα βήματα που επακολούθησαν ήταν ο προσδιορισμός των παραμέτρων του φασματογράφου μάζας (MS) και η επιλογή της μεθόδου προετοιμασίας δειγμάτων, η οποία μετά από εμπλουτισμό του δείγματος σε φωσφοπεπτίδια και nanoLC-MS/MS ανάλυση θα συνείσφερε στην ταυτοποίηση του μεγαλύτερου αριθμού πρωτεϊνών και

πεπτιδίων. Οι εξεταζόμενες μέθοδοι προετοιμασίας δειγμάτων ήταν οι εξής τρεις: Μέθοδος προετοιμασίας με τη χρήση φίλτρων (FASP), μέθοδος προετοιμασίας ενισχυμένη με στερεά φάση (SP3) και πέψη βασισμένη σε τριφθοροαιθανόλη (TFE). Οι πιο κατάλληλες περίοδοι, παράμετροι και μέθοδοι χρησιμοποιήθηκαν στο δεύτερο μέρος της διατριβής, το οποίο περιλάμβανε τη φωσφοπρωτεομική LC-MS/MS ανάλυση εμβρυικών ινοβλαστών ποντικών. Τα κύτταρα αυτά λήφθηκαν από DUSP8-KO ποντίκια που δημιουργήθηκαν με την τεχνολογία CRISPR και από ποντίκια αγρίου τύπου της ίδιας γέννας. Η φωσφορυλίωση των πεπτιδίων εντοπίστηκε σε μεγαλύτερα επίπεδα στην περίπτωση των ινοβλαστών από τα DUSP8-KO ποντίκια. Δεν εντοπίστηκαν σχεδόν καθόλου φωσφορυλιωμένα κατάλοιπα τυροσίνης, πιθανώς λόγω της παροδικής τους φύσεως. Επίσης, παρατηρήθηκε αυξημένη φωσφορυλίωση υποστρωμάτων της κινάσης ERK2 στους ινοβλάστες των DUSP8-KO ποντικών, γεγονός που υποδηλώνει την πιθανή ρύθμιση της ERK2 από την DUSP8. Στο τελευταίο μέρος έγινε συγκριτική ανάλυση του ολικού πρωτεόματος ιστών από DUSP8-KO ποντίκια και ποντίκια αγρίου τύπου της ίδιας γέννας. Τα αποτελέσματα έδειξαν ότι η υπερενεργοποίηση του μονοπατιού των JNK κινασών, λόγω απώλειας της DUSP8 στην περιοχή του εγκεφάλου, πιθανώς οδηγεί σε μιτοχονδριακή απόπτωση και νευροεκφυλισμό. Επιπροσθέτως, η κυτταρική απόκριση στο οξειδωτικό στρες μέσω του μονοπατιού ERK1/2 στην περιοχή του εγκεφάλου των DUSP8-KO ποντικών καθοδηγείται κυρίως από την αυξημένη έκφραση της κινάσης B-Raf, μίας από τις πρωτεΐνες που ταυτοποιήθηκαν στη συγκριτική ανάλυση του ολικού πρωτεόματος.

Acknowledgements

I would like to thank Dr. Panayotou for providing the facilities to conduct the experiments for this thesis and his invaluable advice. I would also like to give my special thanks to Dr. Samiotaki, Dr. Cotsiki and Dr. Stamatakis for their expert assistance, consultation, guidance and patience throughout the research project. Also, many thanks to the members of Kostourou lab in BSRC "Alexander Fleming" for their assistance in cell culture and mouse handling and to the Association of Biomolecular Research Facilities (ABRF) for providing the synthetic phosphopeptide standards. Finally, I am particularly grateful for all kinds of support in this strive provided by my friends and parents in a daily basis.

Table of contents

1. Introduction

1.1 The MAPK Signaling Pathway

Different cell type stimulation experiments in the 1980s with growth factors, such as epithelial growth factor (EGF) and platelet-derived growth factor (PDGF) indicated the predominant presence of a 42 kDa tyrosine-phosphorylated protein[1,2]. Within a time frame close to that study, in different organisms and cell types, tyrosine-phosphorylated proteins of similar masses and behavior with this protein were identified with 2D-gel electrophoresis[3,4,5]. Also, in the same period of time, the insulin receptor tyrosine kinase was being examined based on the hypothesis that its tyrosine phosphorylation activity directly regulated the activity of serine-threonine protein kinases[6,7]. In that study, a 42 kDa serine-threonine kinase, mentioned as mitogen-activated protein kinase (MAPK), was isolated from insulin-stimulated 3T3-L1 cells[7]. MAPK was phosphorylated both in threonine and tyrosine and the scientists were led to the conclusion that it was the same protein that was tyrosine-phosphorylated in response to growth factors in the previously mentioned studies. MAPK was later renamed ERK1 (extracellular signal-regulated kinase 1) by *Boulton et al*[8], due to the great number of extracellular signals able to activate it. The characterization of ERK2 and ERK3 came right next[9], followed by the cloning and biochemical characterization of their upstream kinases in mammalian cells[10]. These studies revealed a conserved regulatory system consisting of a three-level protein kinase activation pathway currently known as the MAPK signaling pathway.

The MAPK signaling pathway is involved in the amplification and integration of a diverse range of signals/stimuli related to multiple cellular processes like growth, differentiation, proliferation, survival, apoptosis, development and immunity[11–17]. The first level out of the three that comprise the MAPK phosphorylation cascade consists of the MAPK kinase kinases (MKKKs). MKKKs are serine/threonine kinases often activated by phosphorylation after interacting with a small GTP-binding protein of the Ras/Rho family in response to extracellular stimuli[18,19]. MKKKs phosphorylate MAPK kinases (MKKs), dual specificity kinases, which are then activated and proceed to

phosphorylate MAP kinases (MAPKs). MAPKs contain a conserved Thr-X-Tyr motif, where both Thr and Tyr residues need to be phosphorylated for the activation of the kinase[14] (Figure 1). After being activated, MAPKs are usually translocated to the nucleus to phosphorylate transcription factors in order to coordinate gene expression. Other targets of MAPKs include MAPK-activated proteins (MAPKAP), such as the 90 kDa ribosomal S6 kinases (RSKs) and the mitogen- and stress-activated kinases (MSKs)[11]. Signaling components involved in the cross-regulation of other pathways, like Sos1 in the Ras/Raf activation mechanism and cytosolic phospholipase A_2 ($cPLA_2$) in eicosanoid biosynthesis are also regulated by MAPK activity. Also, MAPKs phosphorylate cytoskeletal proteins, such as the microtubule-binding protein Tau[20].

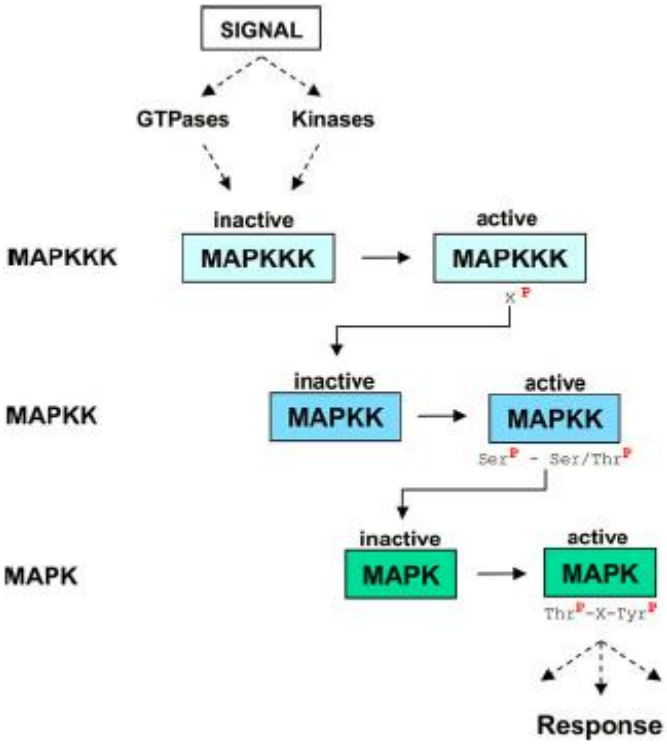

Figure 1: The active (phosphorylated) and inactive forms (dephosphorylated) of the kinases that comprise the three-level MAPK module. Upon activation by different signals, each upstream kinase phosphorylates the downstream kinase, eventually leading to a response, such as the activation of a transcription factor for the regulation of gene transcription. Source: S.F.G. Krens et al. / FEBS Letters 580 (2006) 4984–4990

The three conventional major MAPK subfamilies are the ERK1/2, the c-Jun NH_2-terminal kinases (JNK) and p38 kinases[21–24]. Another MAPK pathway, the MEK5/ERK5, was identified by *Zhou et al*[25]. It shows similarities with the ERK1/2 pathway[26], but also significant differences that make it distinguishable from the other three, such as its involvement in anti-apoptotic signaling and progression of specific cancer types[27–29].

1.1.1 The ERK1/2 pathway

The ERK1/2 pathway is the best characterized MAPK module to date, known for its importance in the regulation of cell proliferation, survival and differentiation, but also in tumorigenesis and other pathological diseases, like neuroinflammation, pain and cardiac hypertrophy[30–33].

The MAPKKKs associated with this pathway are A/B/C-Raf and Raf-1, which are phosphorylated, and thus activated, by MAP4Ks such as Ras, PKA, Rho and Rap1 (Figure 2)[34]. Its MAPKKs are MEK1 and MEK2, while its MAPKs are ERK1 and ERK2[11]. ERK1/2 are activated by phosphorylation in a Thr-Glu-Tyr motif they contain in a specific region called the activation lip. The stimuli are mostly growth and differentiation factors that bind to cell membrane receptors, like receptor tyrosine kinases (RTKs) and G-protein coupled receptors, starting the signaling cascade[20]. The phosphorylation event of ERK1 and ERK2 takes place in scaffolds, proteins that bind to signaling cascade components in different cell compartments. Their role is to regulate the cascade's progression in a spatiotemporal manner[35]. The phosphorylated forms of ERKs either translocate to the nucleus to participate in the activation of various transcription factors or remain in the cytoplasm to regulate other functions (Figure 2)[34].

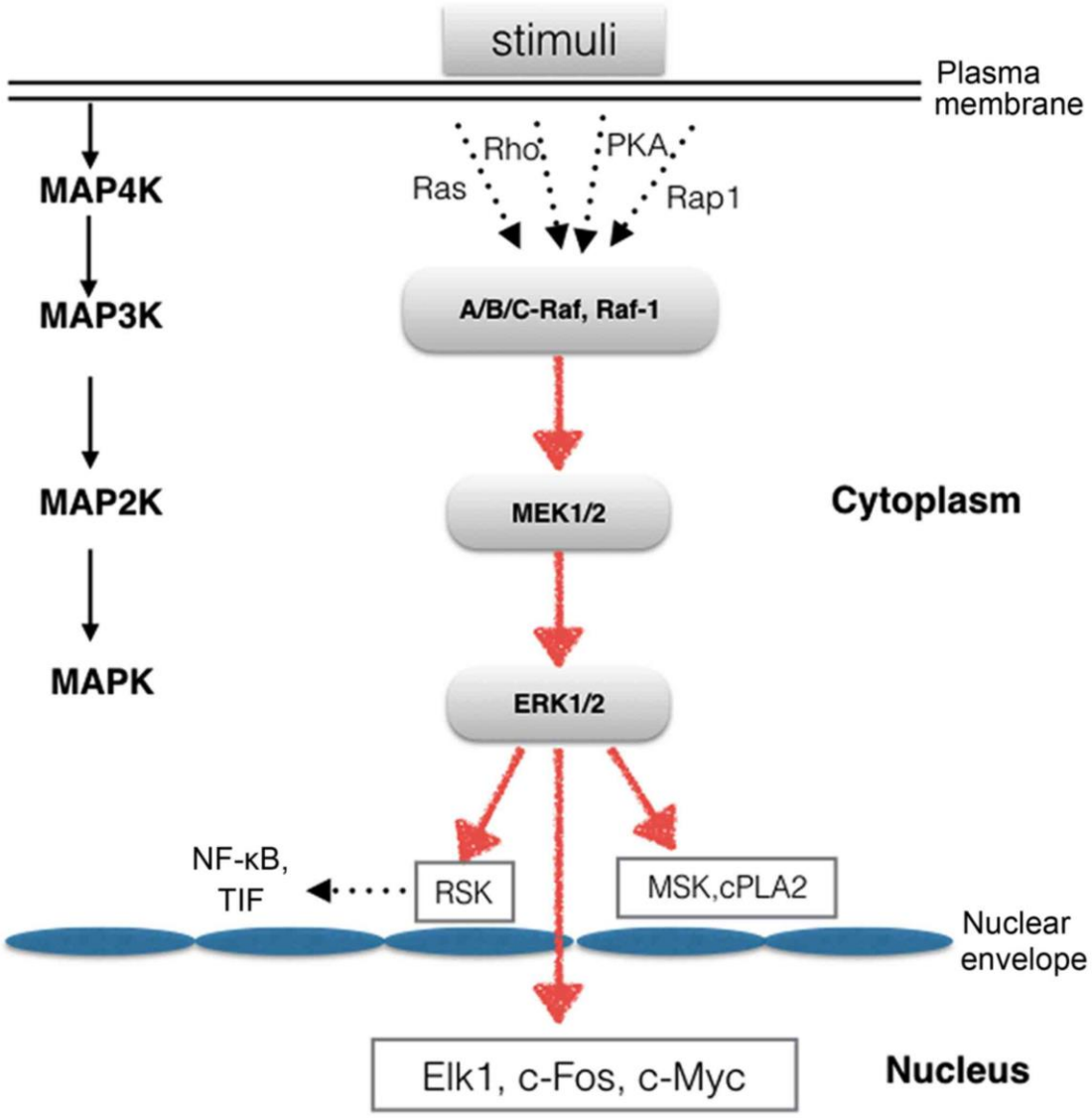

Figure 2: The ERK1/2 MAPK signaling cascade. Source: J. Sun, G. Nan / INTERNATIONAL JOURNAL OF MOLECULAR MEDICINE 39: 1338-1346, 2017

1.1.2 The p38 pathway

The p38 group kinases have been found to be mostly associated with inflammation, cell growth, proliferation, differentiation and cell death[36–40]. The main stimuli that lead to the activation of this specific pathway are UV radiation, osmotic shock, heat shock, DNA damage, inflammatory cytokines, oxidative stress and growth factors[21,38,41].

The MAPKKKs of this pathway include, among others, TAK1[42], DLK/MUK/ZPK[41], ASK1/MAPKKK5[43] and MEKK4[43,44]. These activate the MAPKKs, which consist of MKK3, MKK4 and MKK6[45] (Figure 3), whose role is none other than to phosphorylate the p38 MAPKs p38α (MAPK14)[46,47], p38β (MAPK11)[48], p38γ (MAPK12/ERK6/SAPK3)[49,50] and p38δ (MAPK13/SAPK4)[51,52]. Their dual phosphorylation motif in the activation loop is Thr-Gly-Tyr[53]. Like in the case of the ERK1/2 module, the substrates of the p38 MAPKs are also either nuclear, like transcription factors (e.g ATF-1/2/6, p53, NFAT)[54–57], or cytoplasmic, like Tau[58] or MAPKAPs[41,59].

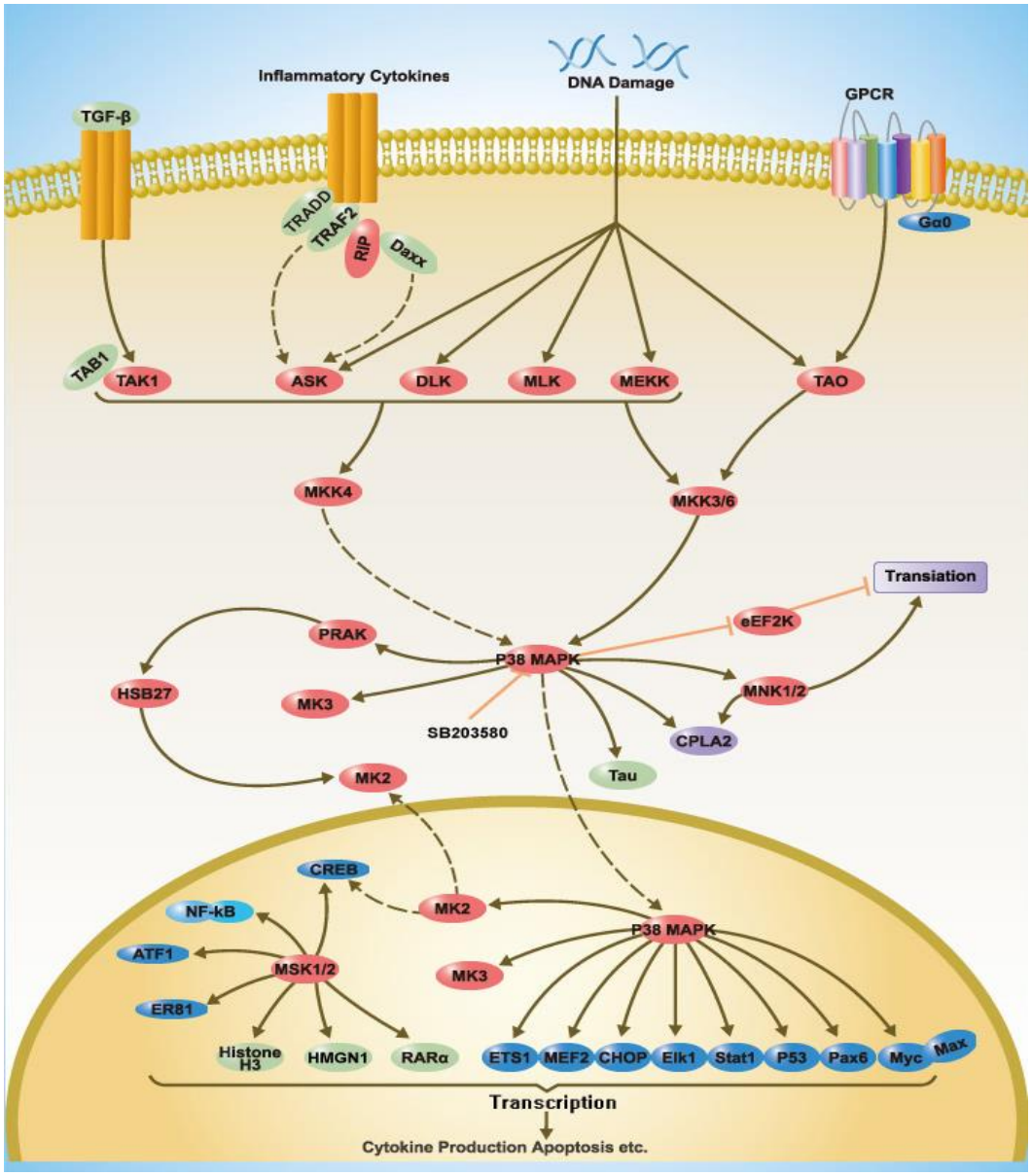

Figure 3: The p38 MAPK signaling cascade. Source: https://www.sinobiological.com/

1.1.3 The JNK pathway

The c-Jun NH_2-terminal Kinase (JNK) pathway is often co-activated and co-regulated with the p38 pathway[60,61]. The major activating stimuli of this pathway are also mostly stress-related like heat, cold, oxidative stress and osmolarity or metabolic changes[16]. Additional stimuli, such as inflammatory cytokines and growth factors are activators of

the JNK signaling cascade, too[62]. This indicates their importance in the regulation of cell growth, differentiation, survival, apoptosis and inflammation.

Among other kinases, the MKKKKs that participate in this pathway are glucokinases (GCKs) and homeodomain-interacting protein kinases (HPKs)[13,63], as shown in Figure 4. Their role is to phosphorylate the large number of MKKKs involved, like MEKK1/4, TAK1 and mixed lineage kinases (MLKs)[60]. The next step on the cascade includes MKK4 and MKK7, which dually phosphorylate the Thr-Pro-Tyr motif in the activation loop of the JNK pathway MAPKs, which are JNK1, JNK2 and JNK3[64–66]. JNK1 and JNK2 isoforms are expressed ubiquitously, while JNK3 expression is limited in the brain, testis and heart[67,68]. Each JNK isoform is associated with distinct functions in different cell types[69–71] and is expressed in two forms, alternatively spliced near the 3' end of the coding region: the short form (46kDa) and the long form (54kDa)[65]. This, along with the alternative splicing of the kinase domain, which generates JNK1α/2α and JNK1β/2β, leads to the expression of more than ten different variants that target distinct transcription factor subsets[72–76]. These transcription factors include c-Fos, c-Jun, ATF2, ELK1, DPC4, p53 and NFAT4 (Figure 4)[77–80].

Scaffolding proteins are really important for the spatiotemporal organization of the JNK signaling cascade as much as for its signaling output. Proteins like the JNK-interacting proteins (JIPs) bind to MKKKs, MKKs, MAPKs and additional proteins through different interaction motifs to bring them together in different cell compartments and regulate the cascade's progression and signal intensity[81–84].

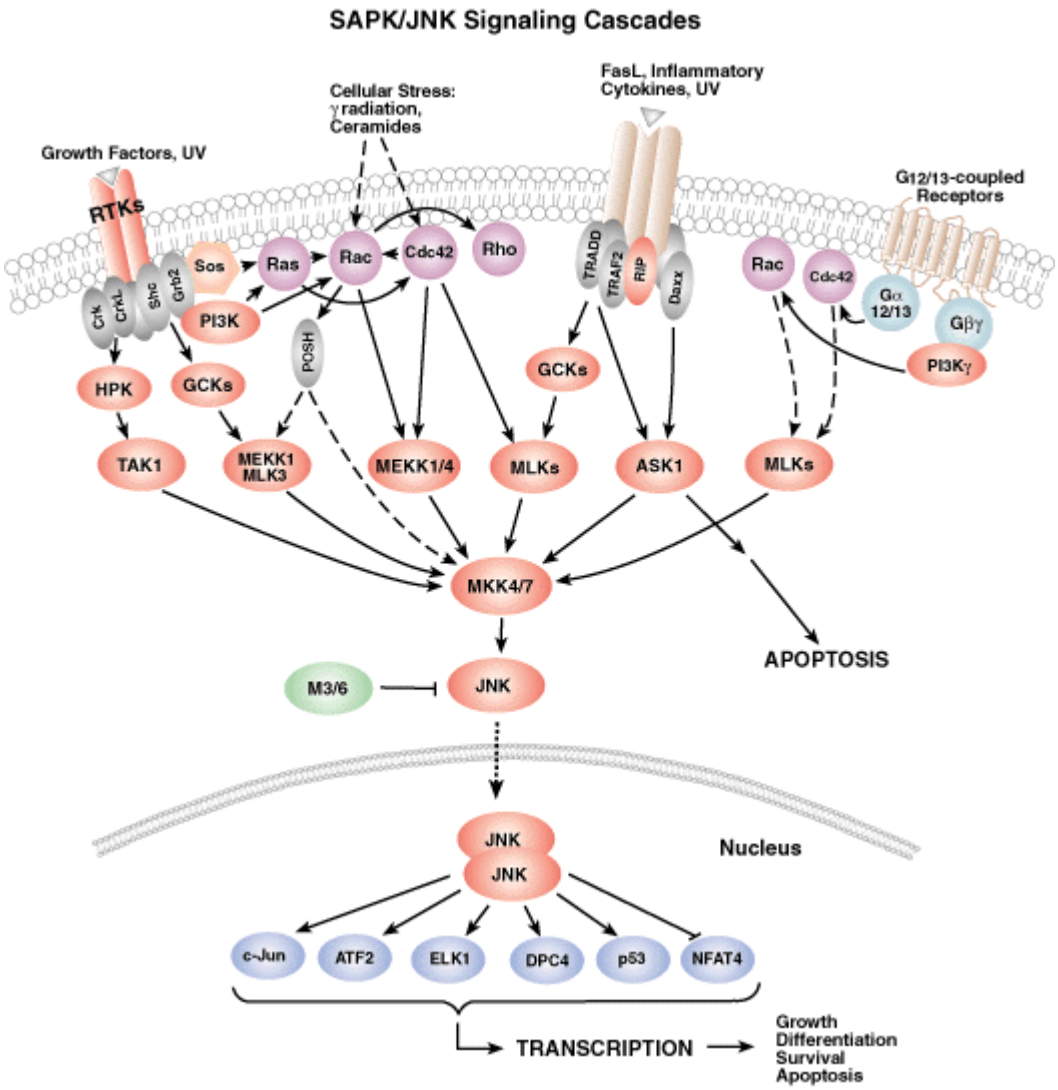

Figure 4: The JNK MAPK signaling cascade.

Source: https://www.ufrgs.br/imunovet/molecular_immunology/sapkjnkmap.html

1.2 Dual Specificity Phosphatases (DUSPs)

Dual specificity phosphatases (DUSPs) are a major subgroup of type-I cysteine-based protein tyrosine phosphatases (PTPs) with the unique trait of being able to dephosphorylate both phosphoserine/phosphothreonine and phosphotyrosine residues in the same substrate[85,86]. Their involvement in a respectable number of different signaling pathways and pathological diseases with distinct characteristics makes them

a truly interesting research topic. Their catalytic mechanism involves the formation of a phosphoryl-intermediate via hydrolysis of the phosphorylated substrate[87].

More than 60 heterogeneous DUSPs, both in structure and function, have been identified. However, there are similarities both in terms of sequence and the presence of specific domains, based on which DUSPs can be categorized into seven different subfamilies: Slingshot phosphatases, phosphatases of regenerating liver (PRLs), Cdc14 phosphatases, PTENs, myotubularins, mitogen-activated protein kinase phosphatases (MKPs) and atypical phosphatases[88].

1.2.1 Mitogen-Activated Protein - Kinase Phosphatases (MKPs)

MKPs constitute a DUSP subgroup that is well characterized. The mammalian group consists of ten proteins able to dephosphorylate specific kinase substrates and negatively regulate their activity. These substrates are MAPKs and the fine-tuning of their activity, by the dephosphorylating action of MKPs, is critical in terms of duration and intensity since both factors affect cellular response. In MAPKs, both their phosphorylated Thr and Tyr residues in their Thr-X-Tyr motif have their phospho-group removed by MKPs. Their ability to remove phospho-groups from both Ser/Thr and Tyr residues in the same substrate possibly stems from their enzymatic pockets being really flexible, which makes them able to accommodate both of the phosphorylated residues[89].

MKPs share a common structure: an N-terminal non catalytic domain and a highly conserved C-terminal catalytic domain[86]. The N-terminal domain contains Kinase Interacting Motifs (KIMs), which are responsible for the specificity of substrate recognition and high-affinity binding[90,91]. KIMs are flanked by two sequences homologous to the Cdc25/rhodanese phosphatase's catalytic site, indicating the common evolutionary origin of MKPs, cdc25 and rhodanese domains[92,93]. There are also sequences that determine the subcellular localization of the phosphatase[94].

Based on substrate specificity, subcellular localization and sequence homology, the MKPs are categorized in three groups: The ERK selective cytoplasmic MKPs (DUSP6/MKP-3, DUSP7/MKPX and DUSP9/MKP-4), the mitogen and stress-inducible nuclear MKPs (DUSP1/MKP-1, DUSP2, DUSP4/MKP-2 and DUSP5) and the

nuclear/cytoplasmic JNK/p38-specific MKPs (DUSP8 (M3⁄6), DUSP10⁄MKP-5 and DUSP16/MKP-7)[95]. Both the distinct domains and categories of MKPs are shown on Figure 5.

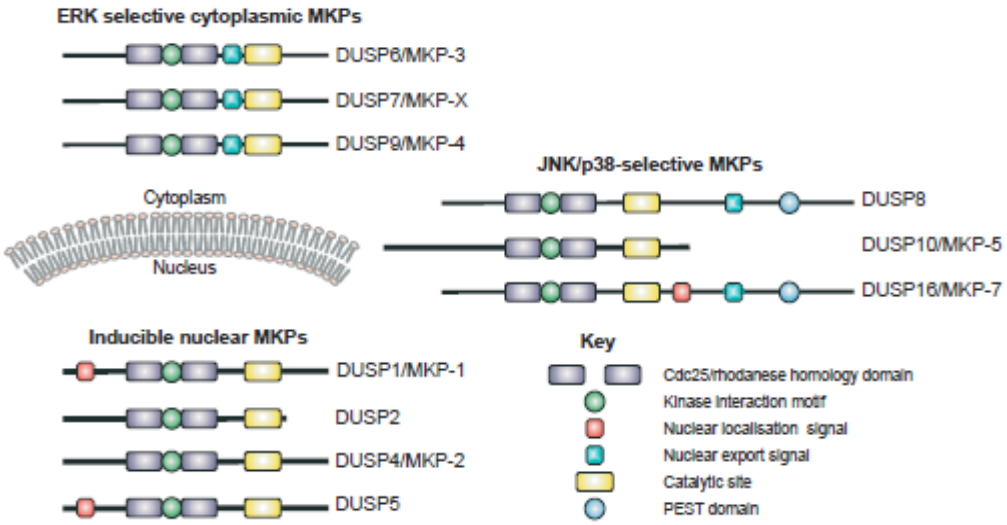

Figure 5: Classification, subcellular localization and distinct domain structure of the MKPs. Source: C.J. Caunt, S.M Keyse / FEBS Journal 280 (2013) 489–504

1.2.2 Dual Specificity Phosphatase 8 (DUSP8)

DUSP8 (the murine orthologue is called M3/6) is the first JNK/p38-selective MKP to be discovered in mammalian cells[96]. It's a 66 kDa protein, localized in both the cytoplasm and the nucleus[95]. The highest RNA transcript and protein levels have been detected in the brain region[97], where it's believed that active DUSP8 plays an important role in neuroprotection against cerebral ischemia[98].

DUSP8 and its human orthologue hVH5, along with DUSP16 which is another JNK/p38-selective MKP contain a PEST-domain in their C-terminus (Figure 5). These domains are sequences rich in proline, glutamic acid, serine and threonine residues. A strongly supported hypothesis is that they contribute to protein degradation signaling, possibly via the proteasome[99]. This could also be associated with the relatively small half-life of the wild-type DUSP8 protein, which is not more than 2h[82,97]. The half-life of DUSP8 is also regulated in the transcriptional level. AUUUA repeats located in the 3' untranslated region of the mRNA transcript contribute to its degradation[100].

Recent work has suggested that DUSP8 interacts with MAP kinases of the ERK1/2 pathway. This interaction seems to play an important role in the cardiomyocytes of mice, since *in vivo* experiments in DUSP8-KO mice and transgenic mice with overexpressed DUSP8 specifically in cardiomyocytes showed protection from heart failure in two surgery-induced disease models and ventricular dilation with greater tendency towards heart failure, respectively[101]. However, the main *in vitro* characterized substrates of DUSP8 mostly include JNK and, to a lesser extent, p38 isoforms[96,102]. These substrates are held together with DUSP8 in scaffolds, such as JIPs, forming a complex that mediates the negative regulation of the signaling cascade. JNK1β and JNK2α seem to show *in vitro* the highest affinity with DUSP8 in resting conditions, but under arsenite-induced oxidative stress there is a differential regulatory response indicated by its enhanced interaction with JNK1α and JNK3 isoforms, instead[103].

As mentioned above, one of the most interesting agents used towards elucidating many dynamic interactions of DUSP8 with different JNK isoforms, is arsenite. Arsenite is a carcinogen, whose action stimulates the production of Reactive Oxygen Species (ROS) inside the cell, creating an oxidative stress state, inhibitory towards DUSP action[104]. Oxidation of a cysteine residue in the catalytic pocket is the most possible explanation for this inhibitory effect[105]. Induction of the JNK and ERK1/2 signaling cascades by arsenite has been found to be associated with apoptotic and carcinogenic effects, respectively[106,107,108]. These opposite biological responses suggest a differential stimulation of the MAPK pathway by arsenite. The underlying mechanism of its action is not yet fully elucidated, but related work suggests a two-way activation of the JNK pathway by arsenite (Figure 6): First, with the activation of ROS-sensitive JNK upstream kinases. Second, with the inactivation of JNK phosphatases, such as DUSP8[104,105,109].

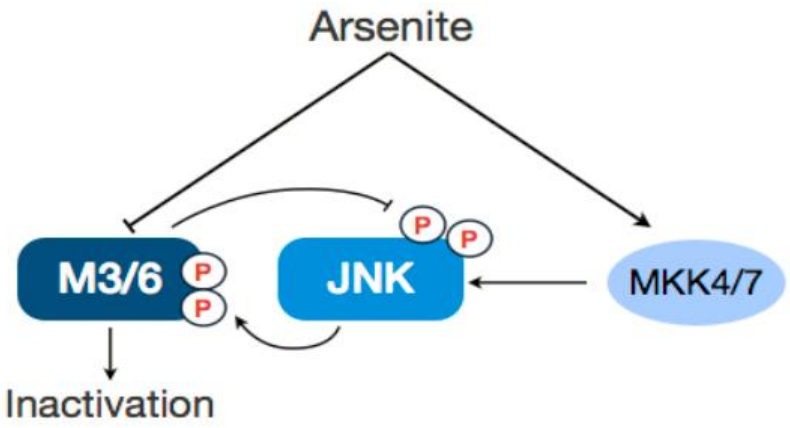

Figure 6: Regulation of JNK and DUSP8 (M3/6) by arsenite-induced oxidative stress

Knockout mouse models in biomedical research are very useful, due to the plethora of advantages they provide for the study of human biology. They are mammals closely related to humans developmentally, behaviorally and physiologically, while almost 99% of their genes have human homologs. Also, many mouse genes are great candidates for accurate and efficient targeted mutagenesis via homologous recombination in embryonic stem cells[110].

In this study, a DUSP8-KO mouse model, generated by the CRISPR-Cas9 method[111], was used. The CRISPR DUSP8-KO mice have an 11bp deletion in exon 2 of the DUSP8 gene, resulting in the formation of a premature stop codon (Figure 7).

5'CACCCCATTGGGTAAGGCATTGGCTCATCCATTCAGGAGGAAGGGCTCAAAGGACATGCCAG
GTGCCAAACACAGGGCCTTCCTGGGAGCCAGCTATAGCTACCCAGATCCCACCATCTGCTGACTA
TTCACCTTTCCCCCAGGTCTGGCACCATGCACTAGGATACCCAGAACGCTGCAAGGCCACGCCCT
CCTCACTTCAGGGGTCACTCTCCCCATTGCCCACCACCCCACCATGGCTGGGGATCGGCTCCCGA
GGAAGGTGATGGACGCAAAGAAACTGGCCAGCCTGCTGCGTGGCGGGCCTGGGGGACCCTTGGT
CATCGACAGCCGGTCCTTCGTGGAGTATAACAGCTGCCACGTGCTGAGCTCTGTGAATATCTGC
TGTTCAAAGCTGGTGAAGCGGCGCCTTCAGCAGGGAAAAGTGACAATTGCTGAGCTTATCCAGC
CTGCTACACGGAGCCAGGTACCTGTGGCCCACCCTTGCATGCGTCTTCAGGGCTGACCATTCCTG
AGCAAACAGACCTATGTCACCTCTGAAAGAGACAGAGGAGCTCCCAGGCCTGGTGCCAAGAGTC
CTCTGATAAGGCATTTCCCCCTCGCTGTCCCTCCGTTCCAAACAGGGTTCCTTGGGGT **3'**

Figure 7: 636 bp coding strand fragment of the DUSP8 gene in WT mice. The blue colored bases are the forward and reverse primers at the 5' and 3' ends that were used for the genotyping. The green colored bases correspond to the start codon of exon 2. The red sequence is the 11 bp deletion that is induced in the CRISPR DUSP8-KO mouse model. This deletion generates the premature stop codon, which the purple-colored bases correspond to.

1.3 Proteomics

Most of the molecular mechanism-elucidating research involving the determination of protein properties, post-translational modification (PTM) states, identification of protein-protein interactions, but also the quantification of proteins that construct complex pathways, such as the MAPK pathway, has been realized with the use of the Western blotting technique for almost 40 years now[112]. The evolution, however, of more high-throughput technologies throughout the past decades has led to the formation of a new era of proteomics, the field that studies the structure, function, expression and interaction of proteins in individual cells up to whole organisms, centered on Mass Spectrometry (MS). The ever increasing accuracy, robustness and reproducibility of MS-related quantitative and qualitative experiments, especially in the last two decades, has made it the current "gold standard" in proteomics studies with Western blotting and related assays now being used mostly for complementary results[113].

1.3.1 Mass Spectrometry (MS)

The term *mass spectrometry* (MS) is used to describe an analytical technique where ions are generated from chemical compounds. These ions are then separated, usually in electromagnetic fields, and detected by their mass to charge ratios (*m/z*) and abundances. These properties are visualized in a spectrum called MS1 spectrum. Ions detected in MS1 spectra are called precursor ions. In a tandem mass spectrometry study (MS/MS), the most abundant precursor ions can be subjected to an extra fragmentation step, generating the MS2 spectra. MS2 spectra contain information about the identification and quantification of the existing peptides in the sample. Depending on the study, multiple fragmentation steps can occur in a mass spectrometry experiment, generating MS^n spectra[114].

Mass spectrometry is usually accompanied with a preliminary step of chromatography, e.g. HPLC, for an initial separation of the molecules that comprise the complex sample and their identification based on their unique properties, like the retention time. The retention time of each compound is the amount of time the respective compound spends

inside the column. After separation through chromatography, the sample is injected into the mass spectrometer[115].

A typical mass spectrometer contains an ion source, a mass analyzer and a detector, all of which operate under high-vacuum conditions (Figure 8). So, after its input, the sample's components are sequentially ionized, separated according to their mass to charge ratio and detected based on the different type of ions produced[114].

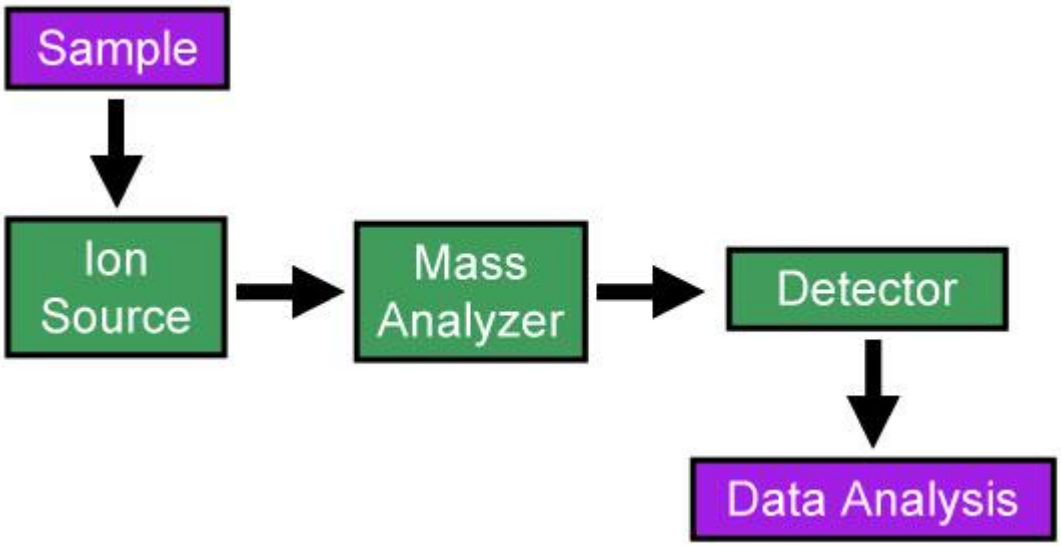

Figure 8: General scheme of a typical mass spectrometer.

Source: dmohankumar.wordpress.com/2011/05/30/mass-spectrometry/

Intact protein studies with MS belong to top down proteomics approaches[116]. These approaches offer the benefit of being able to identify and quantify all modifications simultaneously on the same molecule, information that could be easily lost in digested samples[117]. Bottom-up proteomics, on the other hand, include studies using enzymatically digested samples, usually by trypsin. The mixture's components are then separated with liquid chromatography, ionized with electrospray ionization (ESI) (Figure 9) and then inserted into the mass spectrometer to generate the spectra. The peptides are then identified and quantified using specific software tools. Peptide identification tools are designed for either database or *de novo* search. Choosing the right tool depends on whether the desired search needs to involve all known peptides

presumably present in the sample or focus on sequences with unknown genomic data associated with them, respectively.

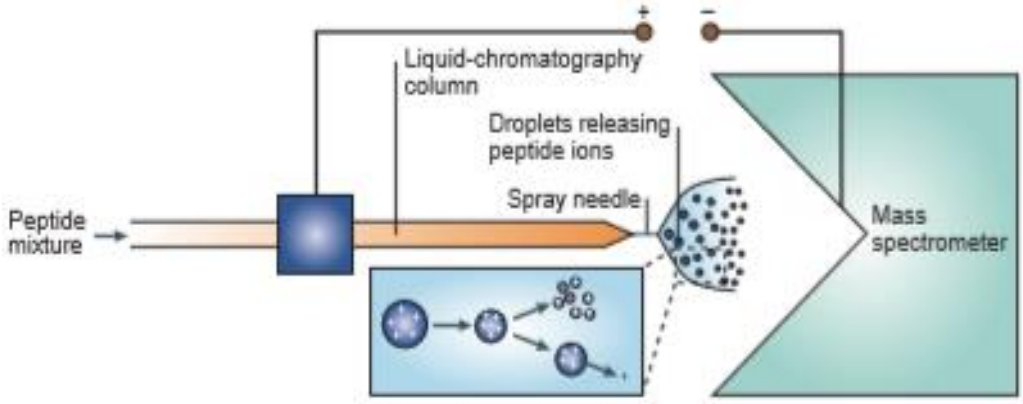

Figure 9: Electrospray Ionization (ESI). The entrance of the mass spectrometer is characterized by a high electrical potential. The eluted peptides from the HPLC column are transferred into the spray needle and become charged droplets, slowly decreasing in size due to solvent evaporation. Ultimately, after many fissions and electrical potential-induced desorption of analyte ions from the droplet surface, each droplet contains one analyte ion on average. Source: Steen & Mann (2004) The abc's (and xyz's) of peptide sequencing. Nat Rev Mol Cell Biol 5:699-711

There are three bottom-up proteomics methods: Data-Dependent Acquisition (DDA), Targeted Proteomics and Data-Independent Acquisition (DIA), with each one having its advantages and disadvantages. DDA methods offer complete proteome coverage in an unbiased way. Precursor ion data and fragment ion spectra are acquired alternatively in order to achieve the isolation and sequential fragmentation of a maximum number of precursors. Quadrupole-Orbitrap analyzers are mostly preferred for these kinds of studies[118]. Targeted proteomics experiments include the sensitive and reproducible acquirement of known proteins of interest. The peptides are isolated by their unique retention time and, after their fragmentation, have their mass analyzed in a triple quadrupole system. The first quadrupole is set to analyze the precursor ions of these exact peptides, while the third is set to analyze the most abundant fragment ions of each known peptide of interest. DIA-based methods, like SWATH[119], require a pre-constructed peptide spectral library. These methods are based on the simultaneous

fragmentation of a large number of precursors and then the extraction of information from multiplexed MS2 spectra, providing a quick analysis of precursor ion masses. Combinations of the best aspects of these three methods in single experiments will probably be a very important concept for the evolution of MS-related proteomics[120].

1.3.2 Phosphoproteomics

Protein phosphorylation, the addition of a phosphate group to the side chain of an amino acid, is a reversible procedure crucially important in the regulation of the majority of cellular processes[121]. Its involvement in a great range of diseases has generated a massive scientific interest around the study of this PTM's localization and extent. The field associated with the large-scale discovery, identification and quantification of phosphoproteins and their phosphorylated sites is called phosphoproteomics[122].

Despite the rapid technological advancements regarding MS-related quantification of PTMs, especially phosphorylation, the most accurate mass spectrometers to date are only capable of identifying 20-40% of the total phosphopeptides in a complex sample. This is due to some main challenges that still remain partially unresolved in the field of phosphoproteomics.

The first, and most important challenge, is the low stoichiometry of phosphorylated proteins. Only a fraction of proteins is phosphorylated at any given time and cellular state and most of them are expressed in relatively low levels. This reduces the efficiency of phosphopeptide identification to a great degree. In order to overcome this, many protocols have been developed focusing on the enrichment of phosphopeptides inside a complex peptide mixture[123]. These protocols often include the use of immobilized metal oxide or metal ion chromatography (MOAC or IMAC, respectively)[124,125], polymer-based metal ion affinity capture (polyMAC)[126], or even the use of antibodies for phosphorylated residues, such as phosphotyrosine, which is the most rarely observed one[127].

The second challenge is the poor ionization efficiency, because the phosphate groups are negatively charged and their binding to the positively charged metal oxides or ions results to their partial or even complete retention[128]. This results also in a poor

fragmentation in the tandem mass spectra due to the formation of uncharged species after ion dissociation, a phenomenon also known as neutral loss[129]. Many strategies have been developed to deal with neutral loss, like the addition of an extra peptide fragmentation step for the neutral loss ion fragments and their subsequent isolation for the generation of the MS^3 spectra. This process is called Data-Dependent Neutral Loss MS^3 ($DDNLMS^3$)[130]. Another approach involves the combination of MS/MS and MS^3 fragmentation, this time without isolation of the neutral loss ion fragments from the MS^2 spectra, so that precursor ion information can be retained and shown, along with the neutral loss ion fragments, in the so called pseudo MS^3 spectra. This method is known as multistage activation[131].

The third and final challenge is the need for the development of more advanced and optimized informatics tools for the assessment, processing and visualization of phosphoproteomics data[132].

All of these challenges were taken into account while conducting the research for the current thesis.

1.4 Aim of the study

The aim of this study was to identify differences in global protein phosphorylation and protein expression due to the deletion of DUSP8 in mice. To achieve this, it was important to first set up a phosphoproteomics workflow, from sample preparation to data analysis using HEK293T cells. Upon completion of the workflow, the aim was to use the identified methods and parameters yielding the most promising results, for a phosphoproteome LC-MS/MS analysis of mouse embryonic fibroblasts (MEFs) derived from WT and DUSP8-KO mice. An additional objective was to gain a perspective on the effects of DUSP8 expression in specific tissues by conducting a comparative whole proteome LC-MS/MS analysis in tissues from wild type C57BL/6 and DUSP8-KO mice.

2. Materials and Methods

2.1 DNA genotyping

2.1.1 DNA extraction

Tails were incubated overnight in Tail Buffer (50mM Tris-HCl pH= 8.5, 10mM EDTA pH= 8.0, 100mM NaCl, 0.2% SDS, 100 μg/mL Proteinase K) at 55ºC. The following day, 6M NaCl was added and the samples were vortexed and centrifuged at 13000 rpm for 20'. Equal volume of isopropanol was added to the soluble fraction and the samples were well mixed with vortexing and centrifuged at 13000 rpm for 20'. The supernatant was discarded and the pellet was washed in 70% EtOH. Samples were then centrifuged at 13000 rpm for 20'. The supernatant was discarded and the pellet was left to air-dry for 15' at RT and then left overnight to dissolve in water for injection (WFI).

2.1.2 Polymerase Chain Reaction (PCR)

1 unit of Q5 HotStart High-Fidelity DNA Polymerase (New England Biolabs) was used for ultra-low error rates in 1X Q5 Buffer (contains 2mM Mg^{2+}). 0.2mM dNTPs (Promega) were also added along with 25pmol of forward and reverse surveyor primers (Invitrogen) and 50-100ng DNA template. Final volumes were reached by adding WFI. The primers contained the following sequences:

Forward surveyor primer (M3/6 exon 1): CACCCCATTGGGTAAGGCAT

Reverse surveyor primer (M3/6 exon 7): CAAACAGGGTTCCTTGGGGT

The reaction took place in a C1000 Touch Thermal Cycler (BioRad) with the following program: Initial denaturation at 98ºC for 30sec and denaturation of each strand at 98ºC for 10 sec. Primer annealing temperature was optimized at 62ºC for 30 sec. Extension reaction by Q5 polymerase followed at 72ºC for 30 seconds and each step

except for initial denaturation was repeated for 34 more times. Final extension of any residual product was done for 2min at 72ºC.

2.1.3 Restriction Enzyme Digestion and agarose gel electrophoresis

100ng of each PCR product were digested by 1 unit of the restriction enzyme SacI-HF (New England BioLabs) in 1X CutSmart Buffer (contains BSA) and WFI. The reaction was mixed, incubated at 37ºC for 1h and terminated by adding 6X Loading Dye (Thermo Scientific) in a final concentration of 1X. The digested products were separated in a 2% agarose gel (1X TAE, 1μg/mL Ethidium Bromide) with GeneRuler DNA ladder mix (Thermo Scientific) as a marker. The gel electrophoresis ran in 120V for 30min.

2.2 Mouse Embryonic Fibroblast (MEF) isolation

Fetal C57BL/6 WT and DUSP8-KO mice were harvested at day 13-14 of pregnancy. Pregnant mice were sacrificed by suffocation in dry ice and cervical dislocation. Fetuses were removed from the uterus and dissected to remove the head, tail and visceral tissues. Tissues were then washed several times with PBS, twice with trypsin, minced well and incubated again in trypsin solution for 5-10min at 37ºC. The trypsin solution was then neutralized with medium containing Dulbecco's modified Eagle medium (DMEM), 10% fetal calf serum (FCS) and 100μg/mL penicillin and streptomycin. Cells were disaggregated and then allowed to sediment. The cell suspension was recovered, followed by spinning at 1000rpm for 5min. Cells were resuspended in medium and plated for culture.

2.3 Cell Culture Techniques

2.3.1 Cell culture and transfection

Human embryonic kidney 293T (HEK293T) cells and mouse embryonic fibroblasts (MEFs) derived from C57BL/6 WT and DUSP8-KO mice were used. Cells were maintained in DMEM, 10% fetal bovine serum (FBS) and 100μg/mL penicillin and streptomycin. All components and media were provided by Gibco. The cells were cultured at 37ºC in a humidified 5% CO_2 atmosphere, grown to confluence and passaged every 3-4 days. Transient HEK293T transfections were carried out using a standard BES Buffer System and calcium phosphate protocol[133]. The WT-myc-DUSP8 constructs subcloned into the pMT-SM vector[134] were provided by Dr. A. Ashworth (Institute of Cancer Research, London).

2.3.2 Cell starvation/stimulation and protein extraction

The transfected HEK293T cells were lysed 48h post-transfection. In the first experiment, WT-myc-DUSP8 transfected cells and control vector-only (pMT-SM) cells were starved for 2h and treated with 250μM arsenite for different time periods (0, 15min, 30min, 60min and 90min). They were lysed with 100mM Tris-HCl pH 7.6, 4% SDS and 50mM DTT, without the presence of protease or phosphatase inhibitors.

In the second experiment, untransfected HEK293T cells were either left untreated or serum starved for different time periods (1, 2, 3, 4 and 24h) and FBS concentrations (0, 0.1 and 1% FBS). They were also treated with 250μM arsenite for 1h. In this culture, cells were lysed with Laemmli buffer (58 mM Tris pH 6.8, 1.7% SDS, 6% glycerol, 0.8% mercaptoethanol, 0.008% bromophenol blue).

HEK293T cells were untreated or treated in large scale preps for MS analysis with either 250μM arsenite for 1h or 20% FBS for 30min. These cells were lysed with 100mM Tris-HCl pH 7.6, 4% SDS, 50mM DTT and cocktails of complete protease and phosphatase inhibitors (Roche). The same lysis buffer was used for the MEFs derived from WT and DUSP8-KO mice from a Het x Het breeding. The MEFs were either left untreated or serum starved (0.1% FBS) for 24h and treated with 250μM arsenite for 1h before lysis.

All extracts were sonicated (BioRuptor) for 15min and centrifuged at 16000xg for 10min at RT. The supernatant was collected.

2.4 Tissue sample preparation

Tissues were isolated from two C57BL/6 WT and two DUSP8-KO mice from a Het x Het breeding. The mice were 11^{th} to 12^{th}-week old. They were sacrificed by suffocation on dry ice. After isolation, the tissues were incubated in liquid nitrogen for 2min and then stored at -80^{o}C. Homogenization was conducted in lysis buffer (100mM Tris-HCl pH 7.6, 4% SDS, 50mM DTT, protease and phosphatase inhibitors) using an OMNI GLH Homogenizer (two 45sec cycles with a 15sec break). The samples were then sonicated (BioRuptor) for 15min (20sec ON, 40sec OFF). Centrifugation followed at 14000xg for 20' at 4^{o}C and the supernatant was collected.

2.5 Bradford Assay for protein concentration determination

The Bio-Rad Protein Assay (Bio-Rad) was used for the determination of protein concentration of cell and tissue extracts. The extracts were first diluted with milliQ H_2O to 1:10 and 1:20, respectively, due to excessive SDS concentration (4%) in the lysis buffer which interferes with the absorbance. A standard curve was created using purified BSA (0.25μg/μL) in different masses (0.5μg, 1.5μg, 2.5μg, 4μg and 5μg). The Protein Dye Reagent Concentrate was diluted to 1:5 and then added to each BSA sample. Incubation occurred for 5min at RT. Absorbance was measured at 595nm and the standard curve of Absorbance (595nm) - Mass was created. The same procedure was followed for the lysates, whose calculated masses from the curve were divided by their measured volumes and then multiplied by the dilution factors to determine the protein concentrations.

2.6 Western blotting

Standard procedures were followed for western blotting. 10-30 μg of total protein were loaded on SDS-PAGE gels. The proteins were then transferred to PVDF membranes (Roche) and blocked in 1% BSA in PBS with 0.05% Tween-20 for 1h. Washes were done with PBS/0.05% Tween-20. Incubation with primary antibodies, diluted in blocking buffer, was done overnight at 4^{o}C. The antibodies used were as follows: Myc-tagged DUSP8 was immunoblotted with the c-myc 9E10 antibody (Santa Cruz). The rest of the antibodies used were the goat anti-DUSP8/HVH5 (Sigma), the mouse monoclonal anti-p-Ser 16B4 and anti-p-Tyr PY99 (Santa Cruz) and the rabbit polyclonal Anti-ACTIVE® JNK (Promega), anti-JNK, anti-p38 and anti-p-p38 (Santa Cruz) antibodies. Mouse monoclonal Pan Actin antibody was used as loading control (NeoMarkers). A goat anti-mouse (Southern Biotech), a goat anti-rabbit (Santa Cruz) and a donkey anti-goat (Santa Cruz) IgG HRP-linked secondary antibodies were used. All blots were exposed using the ECL Plus Reagent for antibody detection (GE Healthcare).

2.7 Protein Digestion Methods

Three protein digestion/sample preparation methods were examined as part of the workflow optimization process: 1) Filter-Aided Sample Preparation (FASP), 2) single-pot solid-phase-enhanced sample preparation (SP3) and 3) trifluoroethanol-based digestion (TFE). FASP is a filter-based digestion method and the lab's current standard method for sample preparation before MS analysis. SP3 is a newly developed process that involves protein digestion on magnetic beads, while TFE-based digestion takes place in-solution. In this study, the digestion enzyme used in all three procedures is trypsin (Trypsin/LysC mix, Promega).

2.7.1 Filter-Aided Sample Preparation (FASP)

The cell lysates and tissue lysates had their proteins denatured in urea (7M Urea, 100mM Tris pH 8.5) and added on top of 10kDa MWCO membranes. The samples were centrifuged twice at 14000xg for 45min. 50mM IAA was then added for alkylation followed by incubation in a completely dark environment for 15min. Samples were then

centrifuged at 14000xg for 30min, urea buffer was added and they were centrifuged again under the same conditions twice. 25mM ammonium bicarbonate (NH_4HCO_3) was added and the samples were centrifuged twice at 14000xg for 45min. After its removal, 1μg trypsin/LysC diluted in 25mM NH_4HCO_3 was added to each sample. Incubation at 37°C and 300rpm overnight followed. The following day the samples were centrifuged at 14000xg for 10min. HPLC Grade water was then added and the samples were incubated for 1h at 37°C and 300rpm. After another centrifugation at 14000xg for 30min, the peptic eluates were left to dry out in a SpeedVac Vacuum Concentrator for 3-4h. The procedure followed according to the FASP protocol is represented in Figure 10.

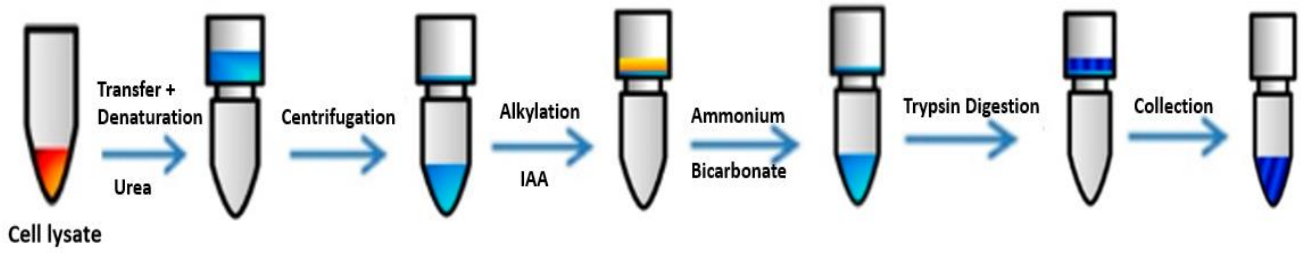

Figure 10: Filter-Aided Sample Preparation (FASP)

2.7.2 Single-Pot Solid-phase-enhanced sample preparation (SP3)

Bead preparation: Sera-Mag SpeedBeads™ Carboxyl Magnetic Beads A and B (GE Healthcare) were combined in a 1:1 volume ratio and diluted in H_2O to a 1:6 ratio. The tubes were incubated on a paramagnetic rack for 2min and then the supernatant was removed. This bead washing step was repeated three times.

Sample preparation: IAA was added to the HEK293T extracts in a final concentration of 15mM, followed by incubation in a completely dark environment for 30min. The reaction was quenched with 20mM DTT. The bead solution was then added to the protein sample using a ratio of 1:10 of bead solution:protein solution. Acetonitrile and formic acid were then added to a final concentration of 50% (v/v) and 0,5% (v/v),

respectively. Incubation at RT for 8min followed in order for the proteins to bind to the beads. After removing the supernatant, the beads were washed with 70% (v/v) EtOH twice and 100% (v/v) acetonitrile once. After the removal of acetonitrile, the protein samples were air-dried for 60s and resuspended in 0.1M NH_4HCO_3 along with 1μg trypsin/LysC. After a 3min sonication in water bath, samples were left for digestion overnight at 37°C and 300rpm. The following day, the samples were centrifuged at 5000rpm for 1min at RT. Sonication for 2min in a water bath followed and the samples were left on a magnetic rack for 2min. The eluate was collected and dried out using a SpeedVac vacuum concentrator for 3-4h. Figure 11 shows a brief schematic of the SP3 sample preparation protocol.

This protocol was improved with the following modifications based on the protocol developed by *Moggridge et al*[135]. 100mM IAA instead of 15mM was added, the bead:protein mix was resolubilized in 50% (v/v) EtOH instead of 50% (v/v) acetonitrile and the beads were redissolved in 200mM NH_4HCO_3 in a 1:50 trypsin/LysC: protein ratio.

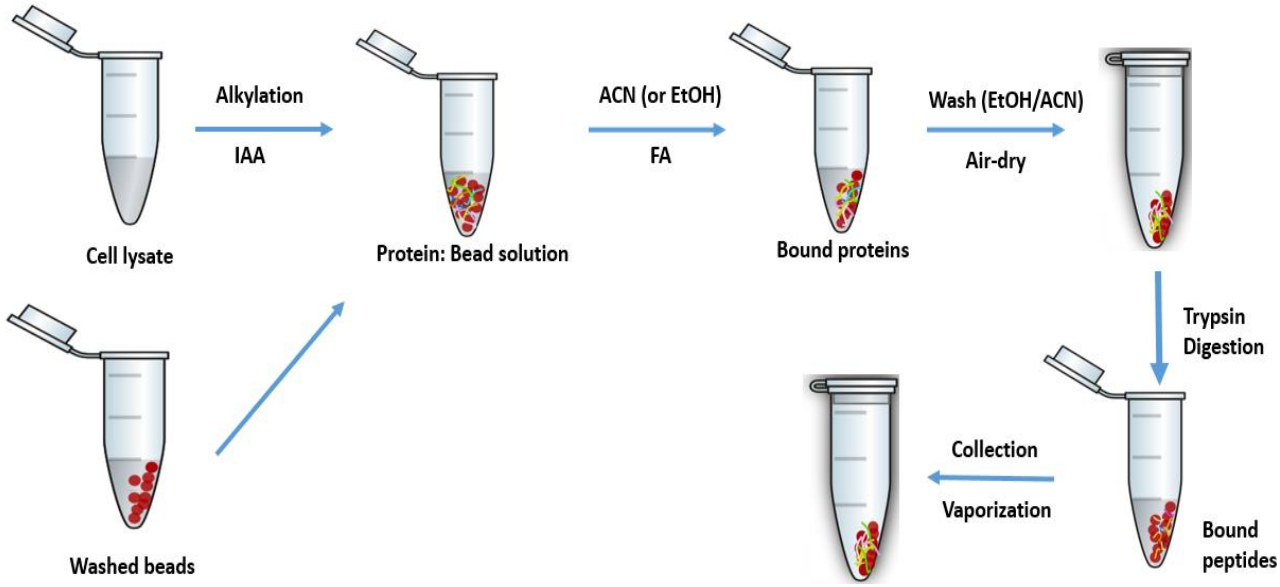

Figure 11: Single-Pot Solid-phase-enhanced sample preparation (SP3)

2.7.3 Trifluoroethanol (TFE) based protein digestion

The procedure followed was based on the protein digestion protocol published by *Humphrey et al*[136]. The lysates were centrifuged for 30min at 3500rpm at 4ºC and the supernatant was diluted 1:1 with milliQ H_2O. 4X volume of -20ºC acetone was added and the lysates were left for precipitation at -20ºC overnight. The following day, the samples were centrifuged for 15min at 2000xg at 4ºC and then washed twice with -20ºC acetone. Pellets were completely broken up during washing by sonication with a BioRuptor at 4ºC. The samples were left to air-dry and then resuspended in TFE digestion buffer (10% 2,2,2-Trifluoroethanol, 100mM NH_4HCO_3). Sonication followed at 4ºC until a homogenous suspension was formed. Protein concentration was determined and samples were diluted to equal concentration in TFE digestion buffer. 1:100 trypsin/LysC mix:protein was added after re-suspending the mix in 0.05% acetic acid/2mM $CaCl_2$. Incubation followed at 37ºC and 300rpm overnight. The following day, the samples were dried out in a SpeedVac Vacuum Concentrator for 3-4h. Figure 12 shows a representative scheme of the workflow followed in TFE-based digestion.

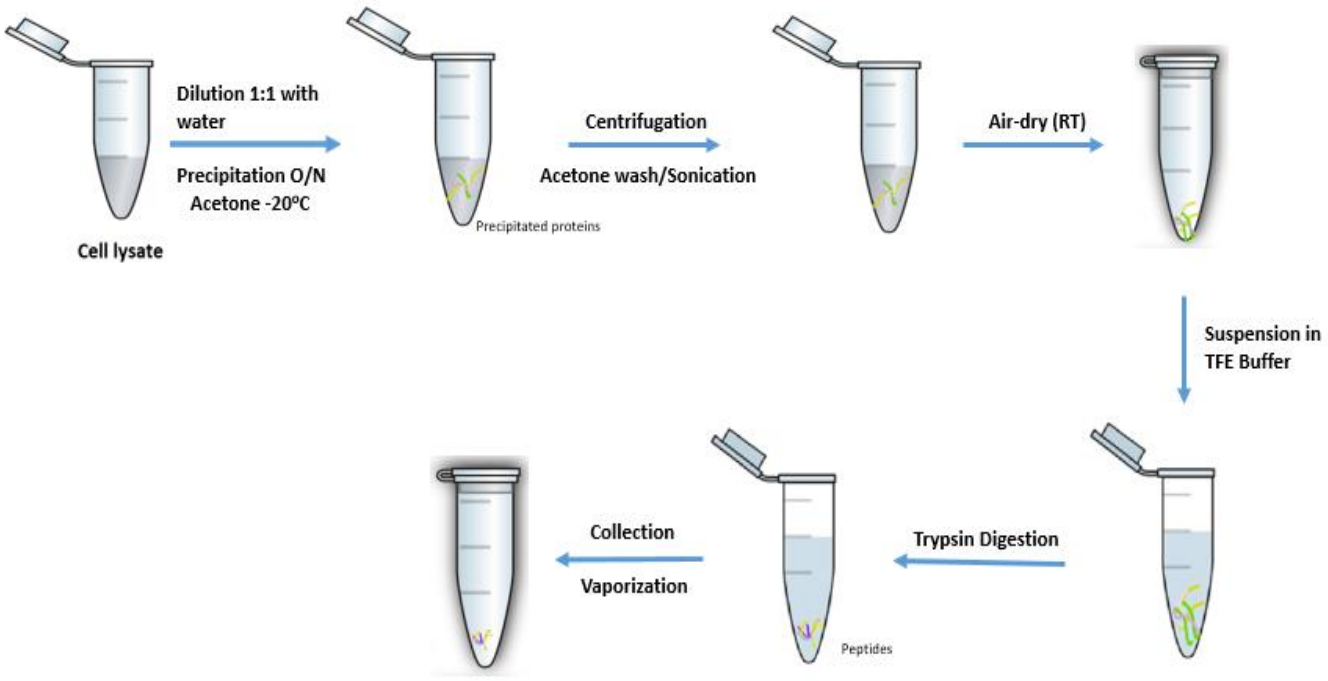

Figure 12: Trifluoroethanol-based protein digestion

2.8 Phosphopeptide enrichment with TiO_2 beads

2.8.1 Phosphopeptide enrichment using magnetic TiO_2 beads

After drying out, the protein samples were solubilized in 80% acetonitrile/ 2% formic acid (FA) and left for 30min at RT to dissolve completely. Phosphopeptide enrichment was carried out with the use of the Thermo Magnetic Titanium Dioxide Phosphopeptide Enrichment Kit (Thermo Scientific) according to the instructions in the kit. The beads were suspended in binding buffer, which, after a 1 min incubation on a magnetic rack, was removed. This magnetic bead preparation step was repeated three times. Protein samples were added to the prepared beads in a ratio of 1:10 (protein: TiO_2 beads) and the mix was incubated at RT for 20-30min. After 1 min on the magnetic rack, the supernatant was discarded. The beads were solubilized in Binding Buffer, left on the rack and then the supernatant was discarded again. This step was repeated 3 times. The beads were then washed with Washing Buffer twice, each time discarding the supernatant after 1 min incubation in the magnetic rack. After the Washing Buffer was completely removed, samples were incubated in Elution Buffer for 10-20min at RT. After a 1 min incubation in the rack, the eluate was collected and dried out in a SpeedVac Vacuum Concentrator for 1h.

2.8.2 Phosphopeptide enrichment using TitanSphere TiO_2 bulk beads

For this phosphopeptide enrichment protocol, TitanSphere TiO Bulk Material 5μm (GL Sciences) was used based on the protocols by *Thingholm et al.*[137] and *Kyono et al*[138]. Empore Disks C8 (GL Sciences) were cut and put at the tips of 200μL pipette tips in order to be used as filters. Titansphere TiO bulk beads (3mg/200μL tip, 5μm, GL Sciences) were stirred and suspended at 80% ACN/0.1% TFA and 300mg/mL lactic acid (solution A). Centrifugation at 2000xg for 2min allowed the beads to bind to the C8 filter. Samples were suspended in solution A and loaded onto the filtered tips-spiked with heavy-labelled phosphopeptides (10pmol/sample) as internal standards (Table 1). After the centrifugation of the tips using the previous conditions, sequential washing with solution A and solution B (80% ACN/0.1% TFA), the phosphopeptidic samples

were eluted with 5% ammonium hydroxide. The eluate was acidified with 5% TFA and concentrated in the SpeedVac evaporator for 2h.

Peptide Name	Peptide sequence	Remark	MW
PhosphoMK10_08	TAGTSFMM-pT-pY-VVT-R*-Qtag	R* = Arg U-13C6, U-15N4	2255.19
PhosphoMK09	TACTNFMM-pT-pY-VVT-R*-Qtag	R* = Arg U-13C6, U-15N4	2328.30

Table 1: Information about the two heavy-labelled phosphopeptides

2.9 NanoLC-MS/MS

After solvent removal through SpeedVac, eluted peptides were reconstituted in a buffer containing 2% acetonitrile and 0.1% formic acid in water. Peptide concentration was determined by measuring the absorbance at 280nm with NanoDrop instrument. 2-3µg peptides were injected in a nano-high performance liquid chromatography system (Ultimate 3000 RSLC, Thermo Scientific) and pre-concentrated on a C18 trap column (Acclaim PepMap100, 100 µm×2 cm, Thermo Fischer Scientific) with a flow rate of 3µL/min. Then, they were loaded online onto a 50cm-long C18 column (75µm ID, particle size 2µm, 100Å, Acclaim PepMap RSLC, Thermo Fischer Scientific). The HPLC solutions were solution A (2% acetonitrile, 0.1% formic acid) and solution B (80% acetonitrile, 0.1% formic acid). Peptide separation was achieved by using a linear gradient of 4% to 40% solution B with a flow rate of 300nL/min. Purified peptides were ionized by a nano-electrospray source and analyzed in an LTQ Orbitrap XL Mass spectrometer (Thermo Fisher Scientific). Data-dependent acquisition (DDA) was used for acquiring full scan MS spectra in the Orbitrap (m/z=300-1600). The resolution was set to 60000 at m/z 400 and automatic gain control target at 10^6 ions. The six most intense ions were isolated and subjected to collision-induced dissociation (CID) and detection in the linear ion trap to acquire the MS/MS spectra. Dynamic exclusion was set to 1min and activated for 90s. Ions with single charge states were excluded. Lock mass of m/z 445,120025 was used for internal calibration. Xcalibur (Thermo Scientific)

was used to acquire the raw files and control the system. For phosphoproteome analysis, Data Dependent Neutral Loss MS^3 ($DDNLMS^3$) and Multistage Activation methods were used.

2.10 Data analysis and visualization

All raw mass spec files were analyzed with ProteomeDiscoverer (v1.4) (Thermo) for the identification, through database matching, of peptides and their corresponding proteins as well as the generation of quantitative data. The complete human reference proteome database was used in the case of HEK293T proteomic analyses.

MEF and tissue raw files were also analyzed with MaxQuant (version 1.6.0.16)[139] using the complete mouse proteome database. Precursor mass tolerance was set at 20ppm, MS/MS fragment tolerance at 0.5 Da and the maximum number of missed cleavages from trypsin was set at 2. The variable modifications for the whole proteome analysis were methionine oxidation, acetylation of the N-terminus and deamidation of asparagine and glutamine. Cysteine carbamidomethylation was set as a fixed modification. Identical variable modifications were set in the phosphoproteome analysis with the addition of Ser/Thr/Tyr phosphorylation and heavy-labelled arginine (Arg10) as variable modifications. The false discovery rate (FDR) was set to 1%. Label-free quantification was carried out and protein abundances were calculated based on the normalized spectral protein intensity (LFQ intensity).

Statistical analysis and data visualization were performed with the Perseus tool (version 1.6.0.2)[140]. Firstly, all potential contaminants, "reverse" and "only identified by site" proteins were filtered out. All LFQ intensities were transformed to log2(x) values. Zero intensities were given random values from a normal distribution (imputation), assuming that the corresponding protein exists in an undetectable quantity in the sample. Replicas were then grouped for each condition (one biological and two technical replicas for the MEFs, two biological and two technical replicas for the tissues). Multiple- and two-sample tests of the grouped proteins were performed using an FDR of 5%. Intensities of statistically significant protein "hits" were normalized with z-scoring. Heat maps were generated after hierarchical clustering and the clusters were used to conduct a Fisher's exact test for enrichment analysis (5% FDR).

For the phosphospecific peptides generated from the MEF samples, an additional filtering step was introduced. The localization probability x was set to $x > 0.75$ (class-I phosphopeptides). The values were log2(x) transformed and sequence specific annotations were added after downloading "Kinase_Substrate_Dataset.gz" and "Phosphorylation_site_dataset.gz" from PhosphoSitePlus (PSP) site. These annotations included the site-specific sequence features, which show in what kind of region the specific site is located (e.g zinc-finger region) and kinase-substrate relations, which link the identified proteins to their corresponding kinases. Additionally, known sites and linear motifs were added to match specific site-containing motifs with kinases and other potential binding partners. The duplicates and triplicates with the same names were grouped and the intensities were imputed by replacing missing values from normal distribution. Multiple- and two-sample tests of the grouped proteins were performed with 5% FDR, intensities were normalized with z-scoring and clustered hierarchically in order to generate the heat map.

.

3. Results

3.1 Phosphoproteomics workflow setup with HEK293T cells

The workflow setup began by identifying the optimal starvation and stimulation conditions (e.g time period under arsenite treatment, FBS concentration for starvation etc.) with western blotting. Three different sample preparation methods were then tested, FASP, SP3 and TFE-based digestion compared in term of the number of identified proteins and peptides upon phosphoproteome analysis with LC-MS/MS. Optimization of mass-spectrometry data-acquisition and bioinformatics analysis parameters was also required. The workflow can be seen in Figure 13.

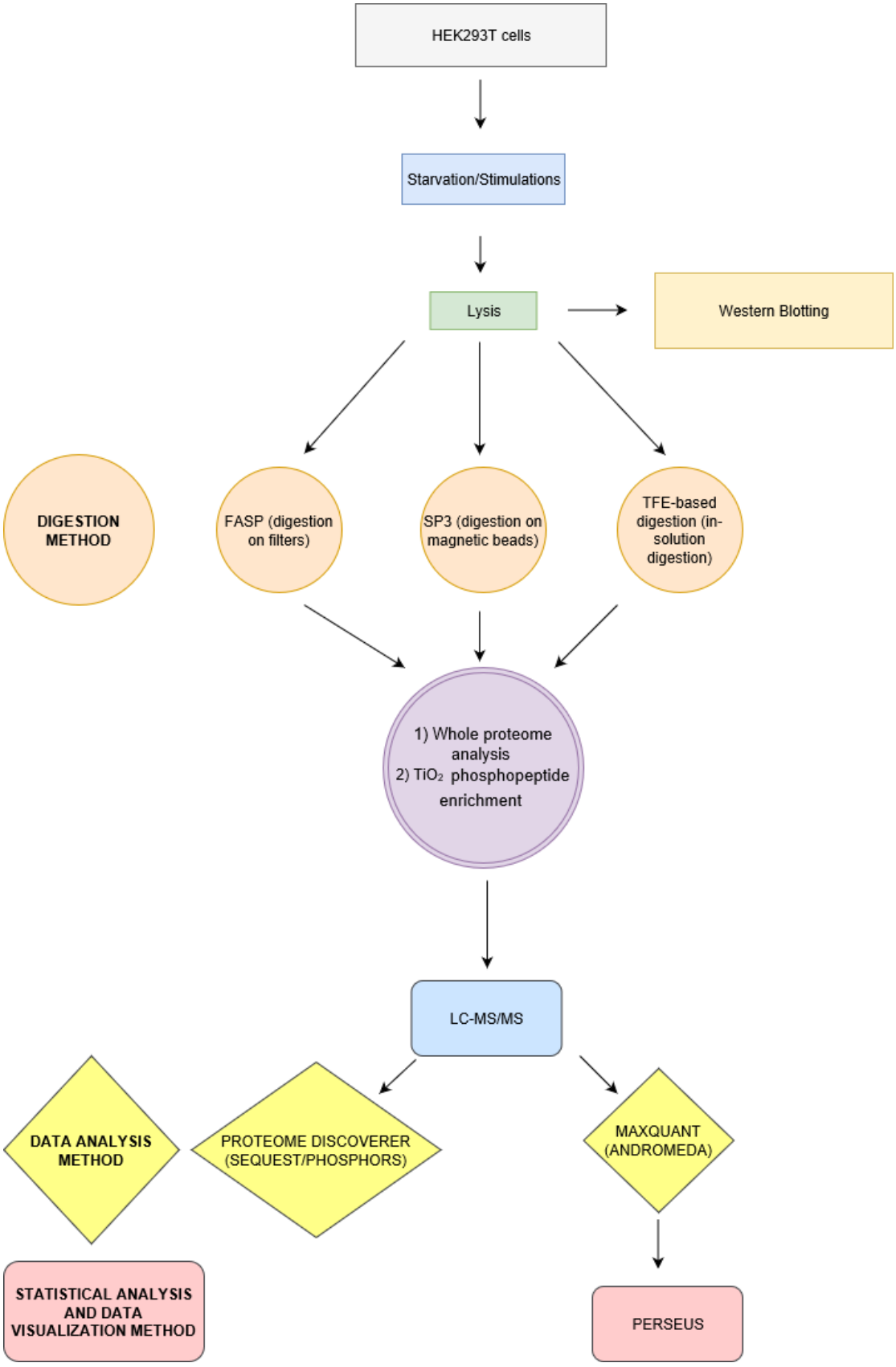

Figure 13: Workflow for the optimization of the methods, conditions and parameters of a whole phosphoproteome analysis protocol, from cell culture to data analysis, using HEK293T cells

3.1.1 Determination of the optimal arsenite treatment period

The first part of the protocol setup was to identify the arsenite stimulation time point in which the effect on DUSP8 expression and phosphorylation levels in DUSP8-transfected HEK293T cells would be clear. Although an overexpression system, it is a useful tool in order to predict the behavior and the regulation of the endogenous protein, which will be investigated in the DUSP8 KO mouse.

Furthermore, another goal was to investigate the activation of JNK, as well as the total serine and tyrosine phosphorylation levels in these same time-points, in order to identify the appropriate time frame for the phosphoproteomic profiling experiments.

In Figure 14, it is shown that the overexpressed transfected DUSP8 decreased over time and began shifting to its phosphorylated form after approximately 60 minutes of arsenite treatment. pJNK levels, on the other hand, gradually increased in both vector-only and DUSP8-transfected HEK293T cells. Cells transfected with the pMT-SM vector only showed generally higher intensities in their pSer and pTyr profiles compared to the DUSP8-transfected cells. An exception to this was the 0 point of arsenite stimulation, where the reverse effect was observed.

Both 60 and 90 minutes of arsenite stimulation showed a clear effect on transfected DUSP8 and pJNK levels. Ultimately, 60min was the chosen time period for arsenite stimulation due to it being the first time point with a clear appearance of the phosphorylated form of DUSP8, as well as a clear activation of JNK and the presence of total serine and tyrosine phosphorylation. In addition, it was preferable to avoid temporally excessive treatment (more than one hour) with an oxidative stress agent capable of causing irreversible damage to the cells and extensive alteration of their proteome, leading to the generation of unreliable results.

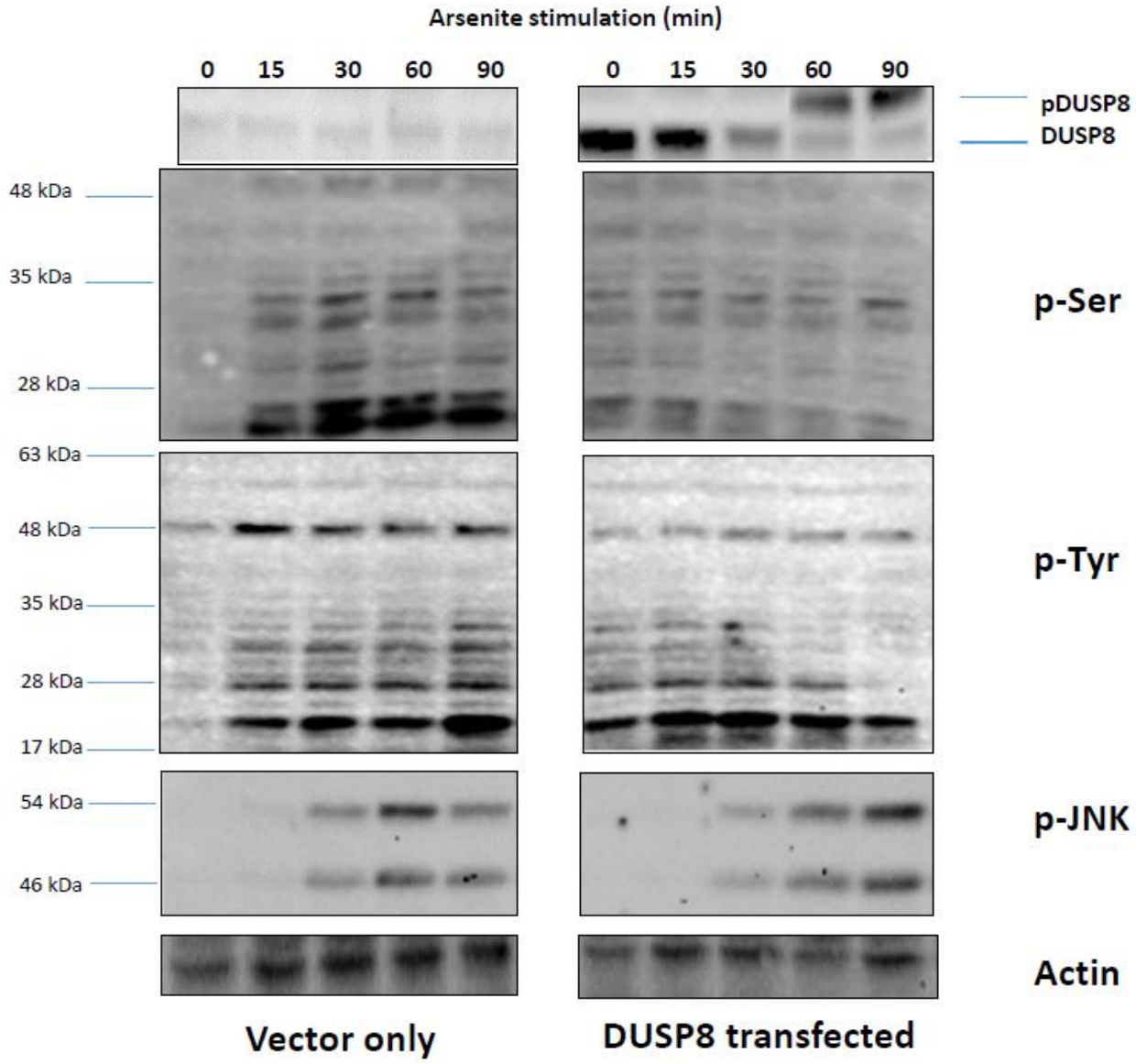

Figure 14: Temporal effect of arsenite on the phosphorylation levels of overexpressed DUSP8, on activation levels of endogenous pJNK and on total serine and tyrosine residues in vector only and DUSP8-transfected HEK293T cells. Cells were starved for 2h and treated with 250μM arsenite for different time periods (0, 15min, 30min, 60min, and 90min). Extracts were analyzed with SDS-PAGE and immunoblotting with the use of an anti-myc antibody for the detection of overexpressed DUSP8, a pJNK-specific antibody for the presence of the activated JNK form and antibodies for the phosphorylated forms of serine and tyrosine residues.

3.1.2 Determination of starvation period and FBS percentage for starvation

Activated JNK levels were examined in different FBS concentrations and starvation periods in untransfected HEK293T cells after 60 minutes of arsenite stimulation (Figure

15). Activation of both p46 and p54 variants was more prominent after one hour of starvation in 0% and 0.1% FBS, compared to longer starvation periods – although still higher than the non-starved control cells. In 1% FBS conditions, pJNK levels were lower and similar to the non-starved control, for any duration of starvation. Also, the difference between the no starvation negative control and the arsenite treated sample show once again the effect of arsenite on JNK phosphorylation.

The best pJNK profiling was the case of no serum and 1h of starvation. However, repeating the cell culture experiments and blotting also with antibodies against pSer and pTyr in different starvation periods led to controversial results (data not shown). Therefore, the HEK293T cell culture for subsequent MS/MS analysis was carried out under no starvation.

In contrast, based on these experiments and further experiments that involved conditioned medium for culture (data not shown), the 24h starvation with conditioned medium was chosen for the culture of MEFs. Conditioned medium has been found to improve the plating efficiency of some cell types, including MEFs[141].

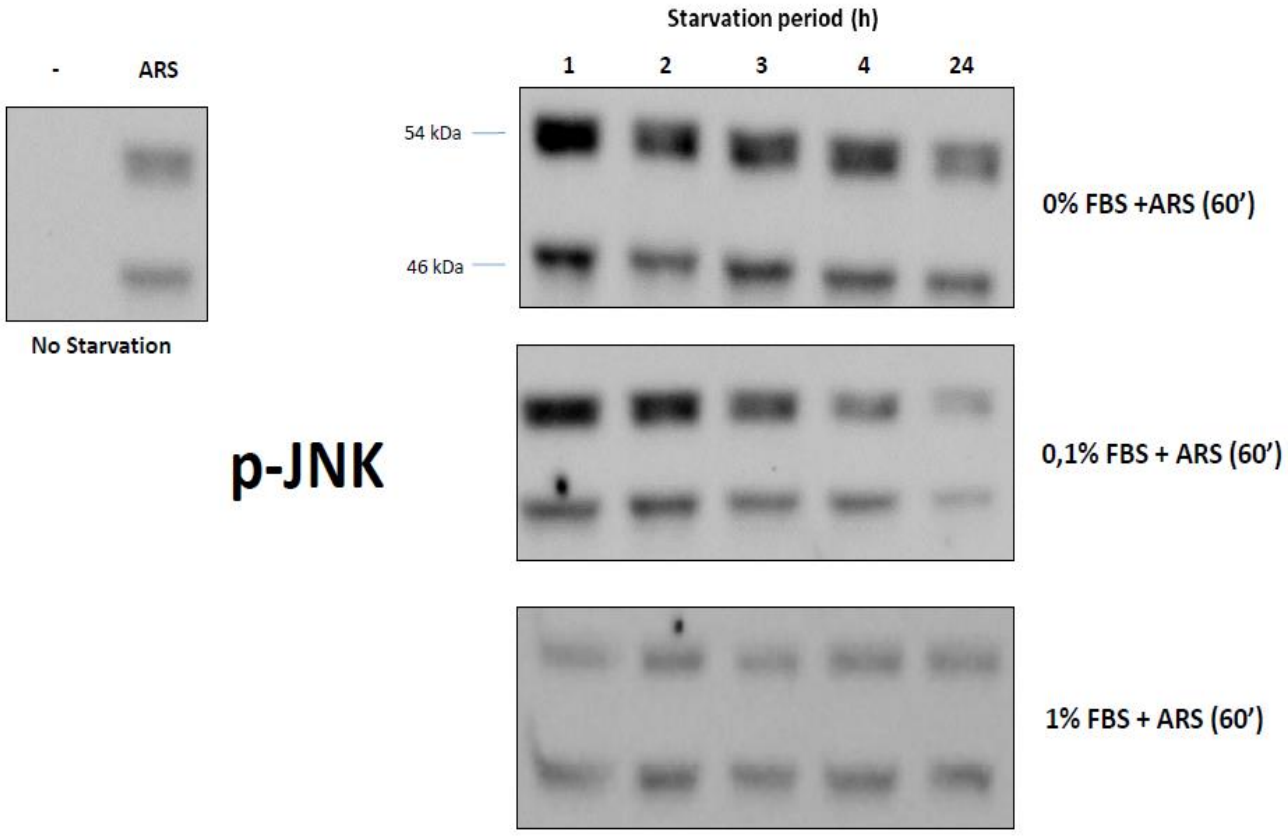

Figure 15: Effect of starvation period and FBS concentration on pJNK levels in untransfected HEK293T cells. The two samples on the left are the non-starved positive and negative controls. Cells were serum starved for different time periods (1, 2, 3, 4 and 24h) and FBS concentrations (0, 0.1 and 1% FBS). They were then treated with 250μM arsenite for 1h. Extracts were analyzed with SDS-PAGE and immunoblotted with a pJNK antibody specific for the activated form of JNK.

3.1.3 Comparison of Multistage Activation (MSA) and Data-Dependent Neutral Loss MS^3 ($DDNLMS^3$) on pure heavy-labelled phosphopeptide standards

There is a variety of methods for the fragmentation of phosphopeptides generating informative and "rich" tandem mass spectra for their complete annotation. In this study, two methods were tested, namely: Multistage activation (MSA) and Data-Dependent Neutral Loss MS^3.

The two methodologies were applied on pure heavy-labelled phosphopeptide standards provided by the ABRF proteomics Standards Research Group (sPRG) as part of their 2018 study for the development of synthetic phosphopeptide standards for MS-based proteomics experiments. A substance is considered heavy-labelled when at least one of its atoms has been replaced by one of its isotopes, which is the same type of atom but with a different number of neutrons. The working standard consisted of a total of 150 heavy-labelled phosphopeptides from proteins involved in 7 different biological pathways: AMPK signaling, death and apoptosis signaling, ErbB signaling, insulin/IGF-1 signaling, mTOR signaling, PI3K/AKT and p38/JNK signaling[142].

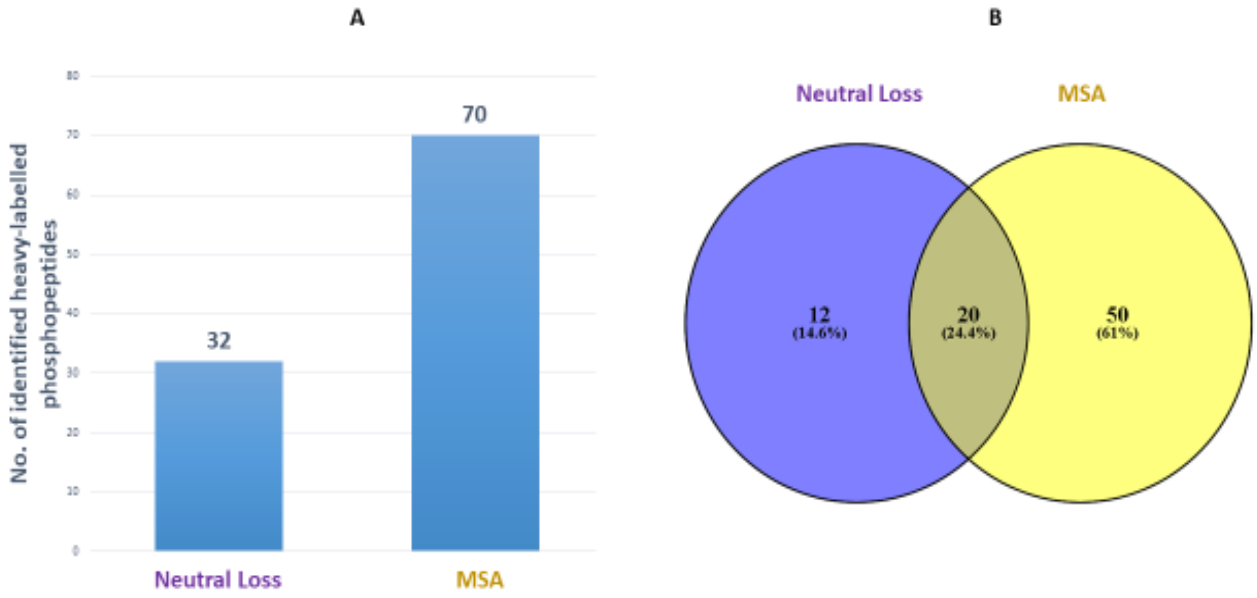

Figure 16: Comparison of DDNLMS3 and MSA. A) Number of identified heavy-labelled phosphopeptides by each methodology. B) Venn diagram showing the numbers of unique and common heavy-labelled phosphopeptides detected by the two methodologies.

With MSA, more than double heavy-labelled phosphopeptides were identified compared to DDNLMS3 (Figure 16A). Also, MSA provided 50 unique identifications, while DDNLMS3 identified only 12 unique phosphopeptides. The common identifications were 20 (Figure 16B).

Except for the number of total and unique phosphopeptides, another way of comparing these two methodologies was by examining the tandem spectra of the same peptide produced by both MSA and DDNLMS3. In Figure 17, the tandem spectra of the peptide with the sequence pSSSSPELQTLQDILGDPGDK are shown. The precursor ion (green) in the DDNLMS3 spectrum contains a phosphogroup. This means that the phosphogroup wasn't subjected to fragmentation, so its fragment ions (b and y) were not generated. However, in the case of MSA, the phosphogroup has been subjected to fragmentation leading to the generation of its subsequent fragment ions. Also, the intensity of the precursor ions is much higher in the case of DDNLMS3, which means that the number of non-fragmented ions is higher and less information is provided.

Additionally, the XCorr of the DDNLMS3 spectrum is 1.68, while the MSA spectrum's XCorr is 2.54. XCorr is the score generated by counting the number of common fragment ions between two different peptides that share the same precursor mass. This number is then used to calculate the cross-correlation score among all candidate peptides of the database in use[143]. A generally acceptable value for XCorr is 2 or more. Less than 2 is considered to be associated with unreliable information.

Detecting more than twice the number of heavy-labelled phosphopeptides and more than four times the number of unique phosphopeptides than DDNLMS3, along with the production of higher quality tandem spectra for most of them, MSA was chosen as the preferred method for phosphoproteomics analysis.

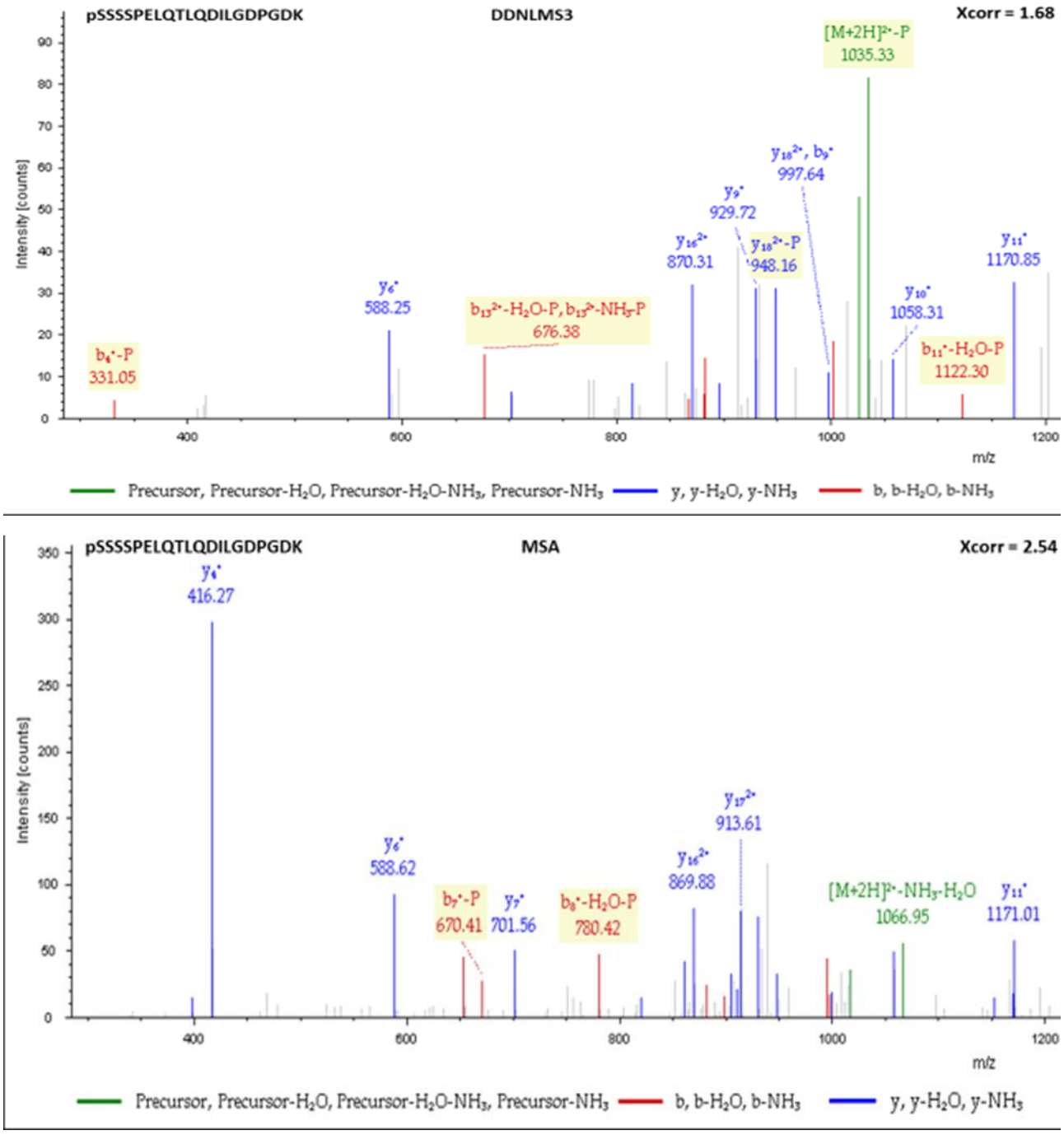

Figure 17: Tandem spectra of the peptide sequence pSSSSPELQTLQDILGDPGDK generated by Data-Dependent Neutral Loss MS3 (top) and Multistage Activation (bottom). The phosphogroup of the detected precursor ion (green) in DDNLMS3 was not fragmented to its respective b and y ions, in contrast to the case of MSA, providing less information about the peptide. Also, the lower XCorr of the DDNLMS3-generated spectrum of this specific peptide indicates the presence of more background noise compared to the MSA-generated spectrum.

3.1.4 Comparison of FASP, SP3 and TFE-based digestion on HEK293T samples

The results from the MS analysis of the enriched phosphoproteome of control, FBS- and arsenite-treated HEK293T cells were initially supposed to be examined individually per condition. However, due to poor data being generated this way, the results were pooled together so that the choice of the preferred sample preparation/digestion method would be as reliable as possible.

The following histograms show the number of proteins, peptides, phosphorylated peptides (Figure 19) and total Peptide Spectrum Matches (PSMs) (Figure 18) identified with ProteomeDiscoverer in the differently prepared protein digests of HEK293T samples. PSMs essentially correspond to the identification frequency of a specific peptide sequence.

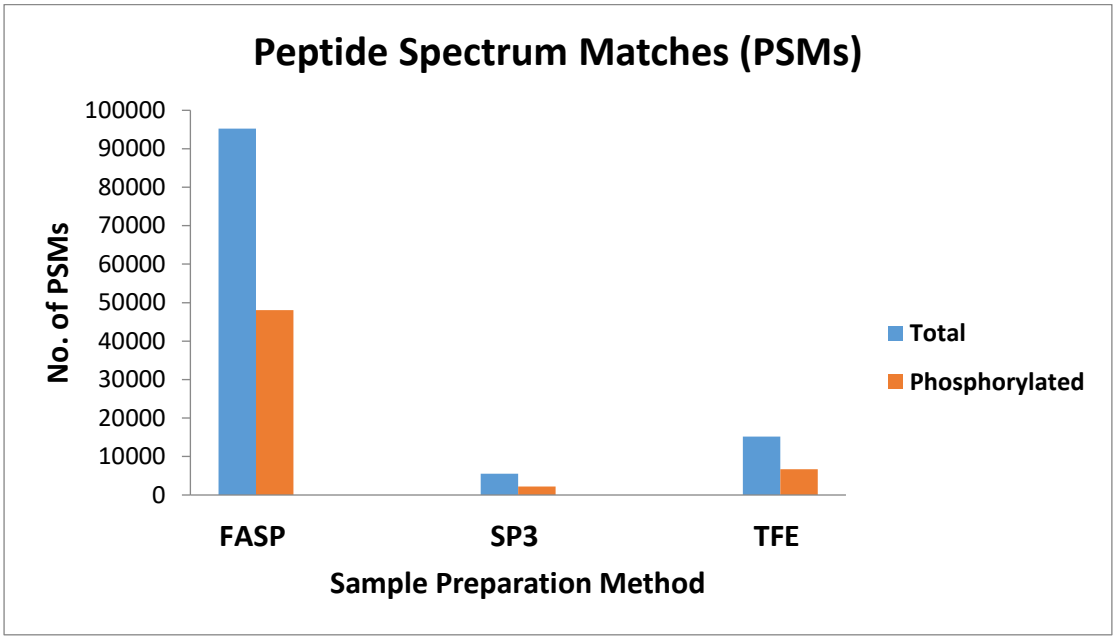

Figure 18: Number of identified Peptide Spectrum Matches (PSMs) for total and phosphorylated peptides in FASP, SP3 and TFE-based preparation of control, FBS- and arsenite-treated HEK293T cells from phosphoproteome MS analysis.

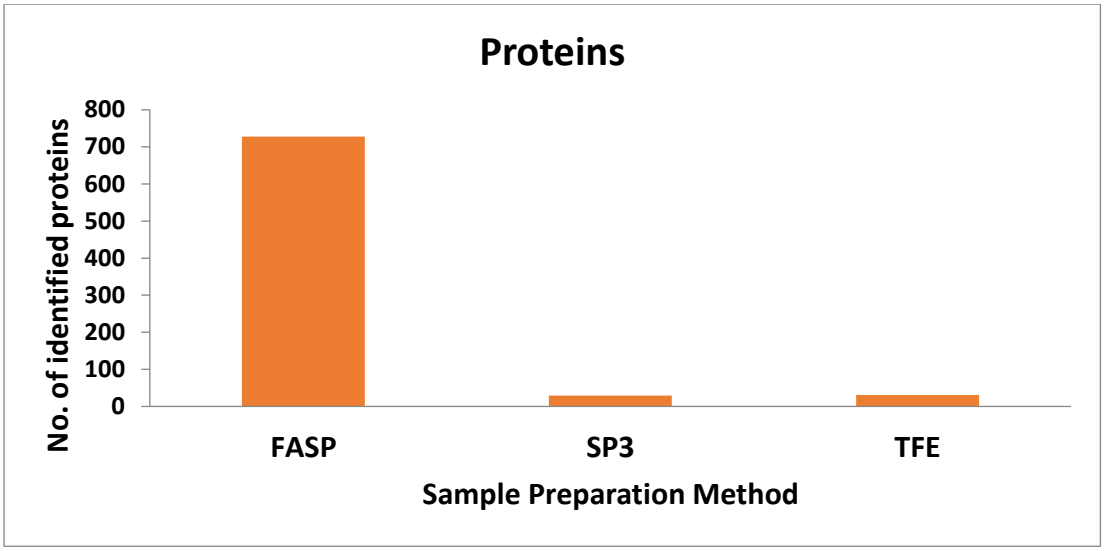

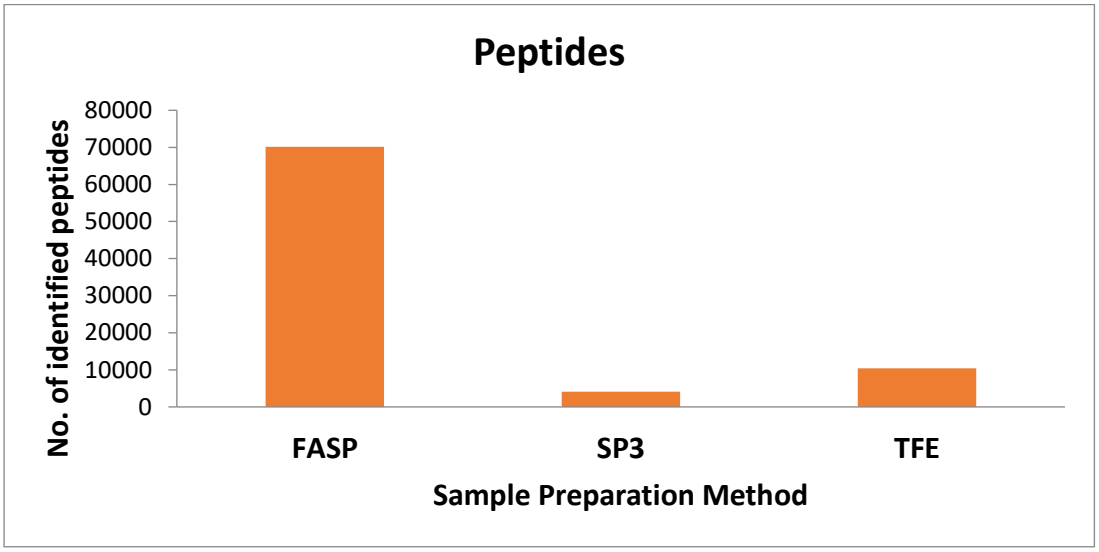

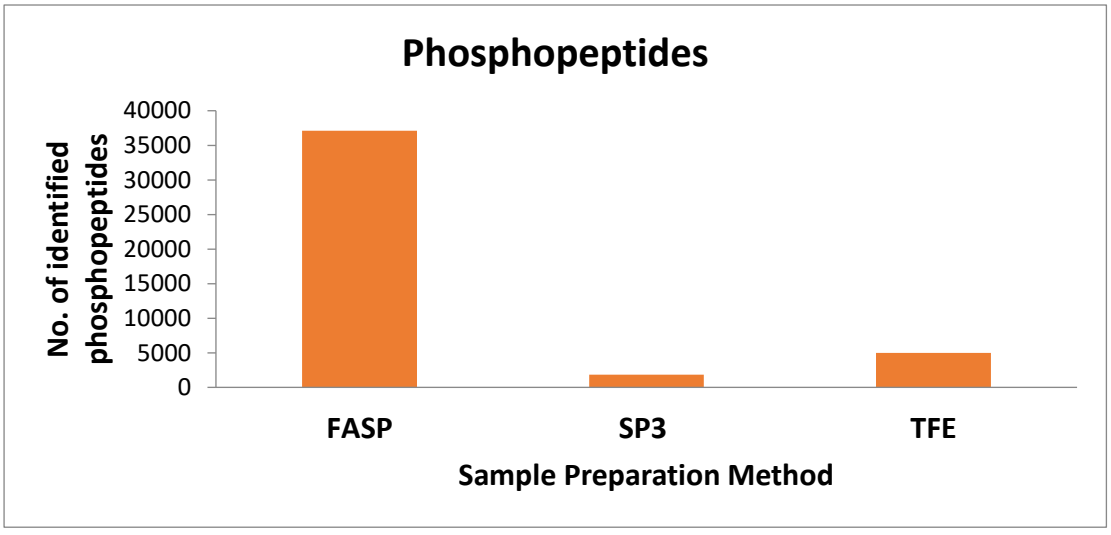

Figure 19: Number of identified proteins, peptides and phosphorylated peptides in FASP, SP3 and TFE-based preparation of control, FBS- and arsenite-treated HEK293T cells from the phosphoproteome MS analysis.

The FASP method for protein sample preparation showed a generally higher protein, peptide and PSM yield compared to the other two methods. TFE-based preparation showed the second best results, whereas SP3 showed the least remarkable performance. So, it was decided that FASP should be the method used for both MEF and tissue sample preparation for this project.

3.2 Genotyping and phosphoproteome LC-MS/MS analysis of MEFs derived from DUSP8-KO and WT mice

3.2.1 DNA genotyping of wild-type, heterozygous and DUSP8-knockout mice for MEF isolation

The undigested PCR product was the 636bp fragment shown in Figure 7. The restriction enzyme SacI has two restriction sites in the WT and one restriction site in the KO allele, since one of these sites is located in the 11 bp deleted sequence. Thus, three fragments are generated in the case of WT mice (371, 185 and 80bp), two fragments in KO homozygotes (545 and 80bp) and four fragments in heterozygotes (545, 371, 185 and 80 bp), since they contain both WT and KO alleles (Figure 20).

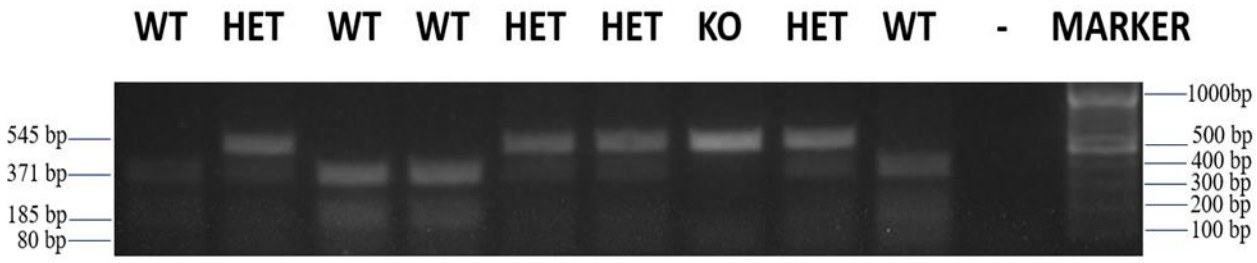

Figure 20: Agarose gel (2% w/v) of the SacI-restricted PCR-amplified Dusp8 gene fragment. Restriction by SacI generates three fragments in WT mice (371, 185 and 80bp), two fragments in KO homozygotes (545 and 80bp) and four fragments in heterozygotes (545, 371, 185 and 80 bp).

From the gel in Figure 20, it's shown that we had 4 WT, 4 heterozygotes and 1 DUSP8-KO mouse in that litter. MEFs were derived from one WT and the KO mouse.

3.2.2 Phosphoproteome analysis of WT and DUSP8-KO arsenite-stimulated mouse embryonic fibroblasts

Phosphoproteome analysis of FASP-treated and phosphopeptide enriched MEFs derived from the WT and DUSP8-KO mice yielded 1900 proteins with 201 statistically significant phosphorylated sites, whose differential intensities can be seen in the heat map (Figure 21A). KO samples showed a general upregulation in distinct site phosphorylations. Out of these sites, 84.1% were serine, 15.4% were threonine and only 0.5% were tyrosine residues (Figure 21B). These sites were then examined based on which kinase phosphorylated them using the "Substrate-Kinase Relations" database from PhosphoSitePlus. Due to being relatively new, the database is still constantly expanding, so the resulting number of kinases was low.

The kinase with the most substrates identified was ERK2 (Figure 22A). The volcano plot in Figure 22B shows the gene names of the ERK2 substrates detected in the arsenite-stimulated MEFs. Each dot corresponds to a specific phosphopeptide of that substrate. The fact that some names appear twice is due to the specific phosphopeptide being detected with single or multiple phosphorylated sites.

Control versus arsenite stimulation was also tested in both conditions separately (data not shown). Both KO and WT arsenite-stimulated MEFs showed higher overall phosphorylation intensities compared to the control, unstimulated cells.

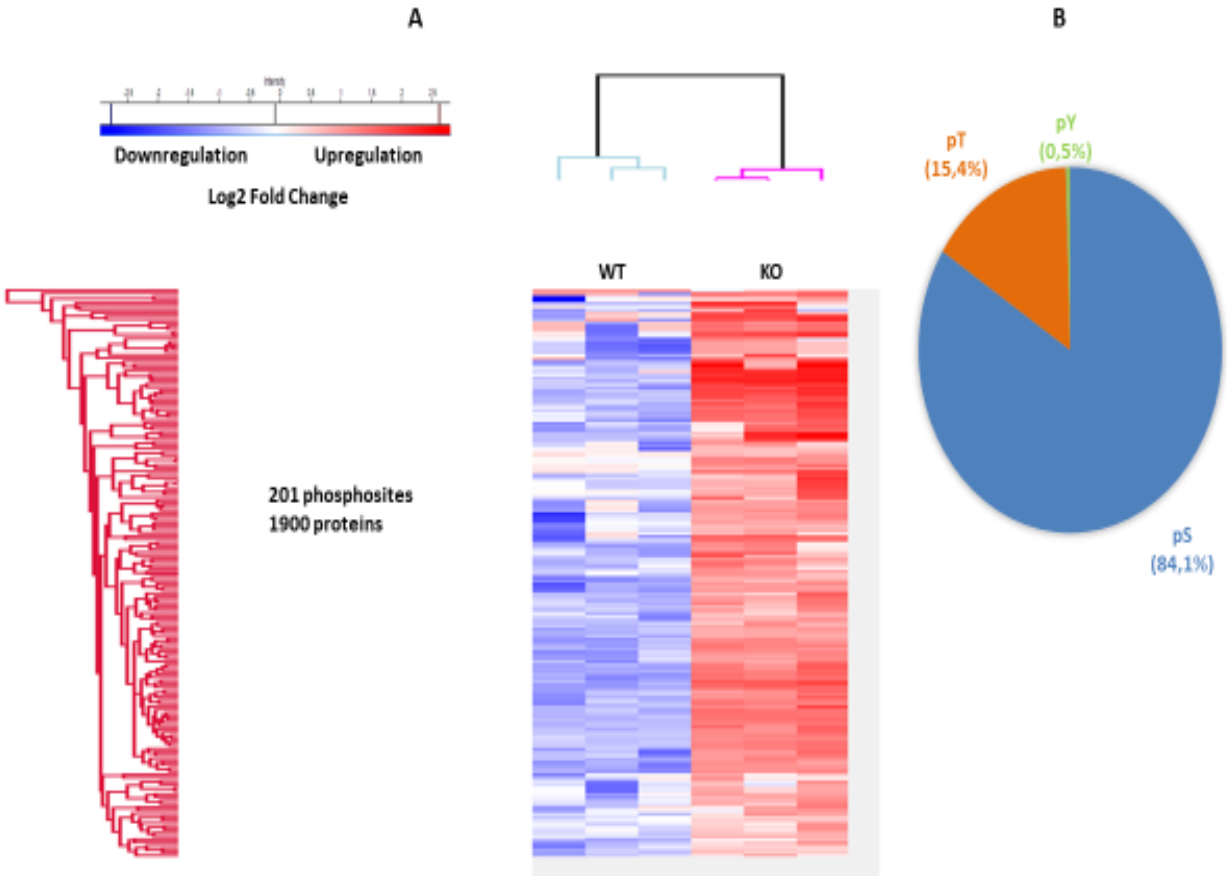

Figure 21: A) Heat map showing the phosphorylated site intensities in arsenite-stimulated MEFs derived from WT and DUSP8-KO mice. One biological replicate was used for each condition with two more technical replicates each. Potential contaminants and "reverse" hits were filtered out. The remaining intensities were log2 transformed, grouped and had their NaN (Not a Number) values replaced by normal distribution values. A two-sample Student's t-test was carried out and statistically significant intensities were normalized by z-scoring and clustered hierarchically. B) Percentages of the 201 statistically significant phosphosites. 31 (15,4%) pT (threonine), 169 (84,1%) pS (serine) and 1 (0,5%) pTyr (tyrosine) residues were identified.

A

Kinase	Number of Substrates
ERK2	5
P38A	1
mTOR	2
CK2A1	2
PAK4	2
DAPK1	2
MKK6	1

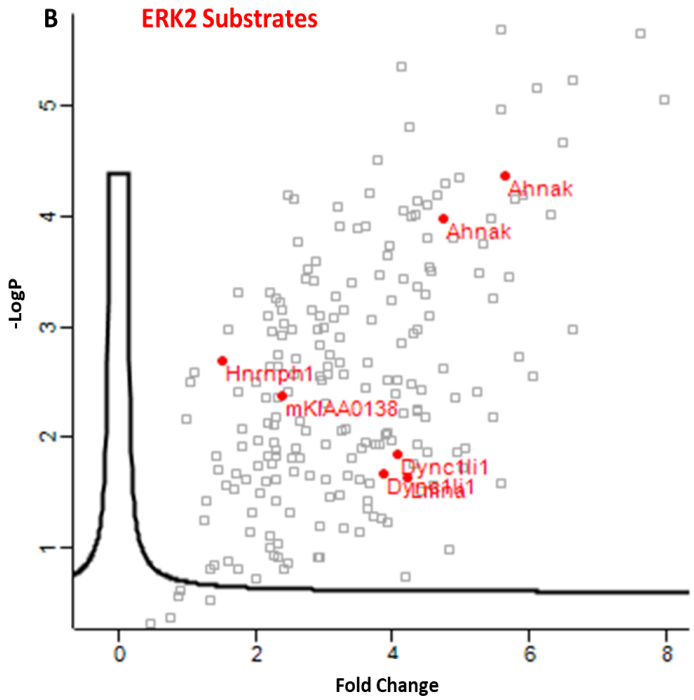

Figure 22: A) Table showing the identified kinase-substrate relations in arsenite-stimulated MEFs from WT and DUSP8-KO mice. The Kinase-Substrate annotation was downloaded from PhosphoSitePlus. B) Volcano plot showing the gene names of the identified substrates of ERK2 kinase. Each dot corresponds to a specific phosphopeptide of the substrate. This phosphopeptide may be phosphorylated in one or more sites, which may cause its detection to happen twice The x-axis represents the log2 fold change of each phosphopeptide's intensities between the WT and KO samples, while the y-axis represents the negative log10 p-value for each phosphopeptide.

3.3 Detection of JNK activation and comparative whole proteome LC-MS/MS analysis of tissues from DUSP8-KO and WT mice

3.3.1 Comparison of basal pJNK levels in tissues of WT and DUSP8-KO mice

Basal pJNK levels in the brain area of DUSP8-KO mice were considerably higher than WT mice in both p46 and p54 variants (Figure 23). Total JNK was detected in the same levels among all replicates. Average pJNK values of the two replicates for each variant were calculated and normalized to the average actin value of the WT mice. In kidney blots, neither of the pJNK variants were detected (data not shown).

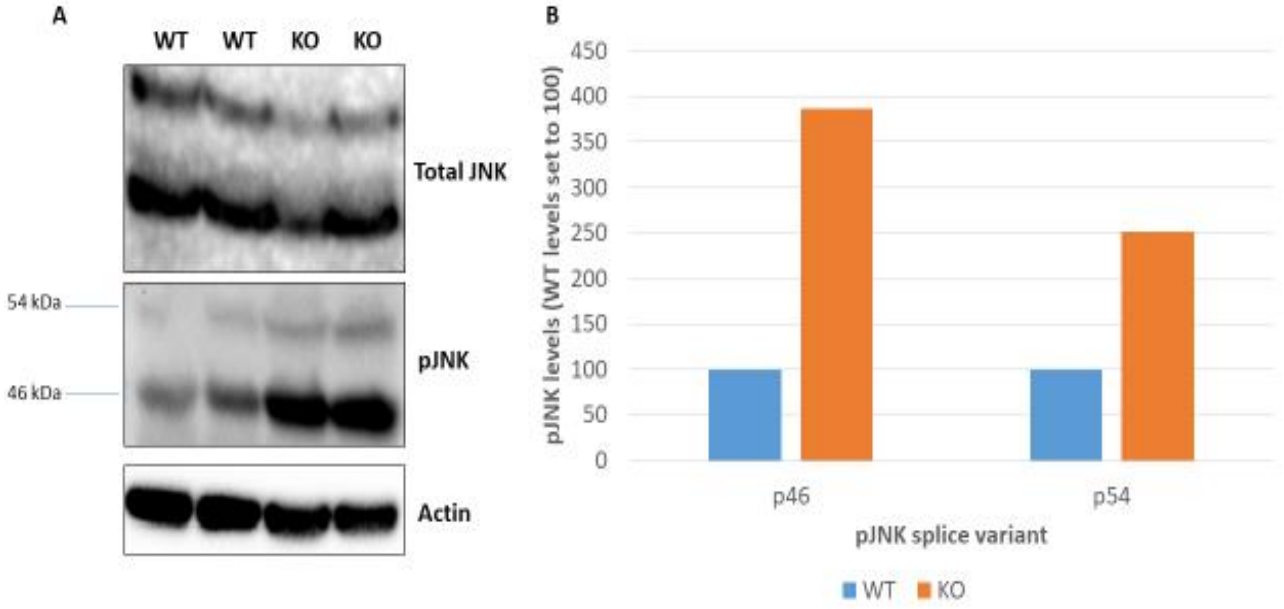

Figure 23: A) Total JNK and pJNK levels in the brain tissue of WT and DUSP8-KO mice. Homogenates were analyzed with SDS-PAGE and immunoblotting with the use of a JNK antibody for the detection of the total JNK forms and a pJNK-specific antibody for the presence of the activated pJNK forms. B) Histogram showing the relative levels of the two pJNK splice variants, p46 and p54, in the brains of WT and DUSP8-KO mice. Average pJNK values of the two replicates for each variant were calculated and normalized to the average actin value of the WT mice.

3.3.2 Whole proteome analysis of brain and kidney tissues of DUSP8-KO mice

Kidney whole proteome analysis revealed only five proteins that were differentially expressed statistically significantly different between WT and DUSP8-KO mice (data not shown), thus preventing any further analyses.

On the contrary, the whole brain proteomes of WT and KO mice exhibited significant and interesting differences. The heat map generated by hierarchical clustering of the protein LFQ intensities in the brain showed two distinct profiles between WT and KO samples (Figure 24). Two main clusters of differentially regulated protein groups were generated and classified. In the upper cluster (774 proteins), most differentially expressed proteins were upregulated in the KO samples. In the lower cluster (343 proteins), most of them were downregulated in the same samples. The clusters underwent Enrichment Analysis using Fisher's Exact Test. The 4 most significant KEGG pathways (Parkinson's disease, Huntington's disease, oxidative

phosphorylation, Alzheimer's disease) are shown in Table 2. All 4 KEGG pathways were associated with more than 30 genes and had enrichment factors above the value of 1. This means that more genes than normal were involved in these cases.

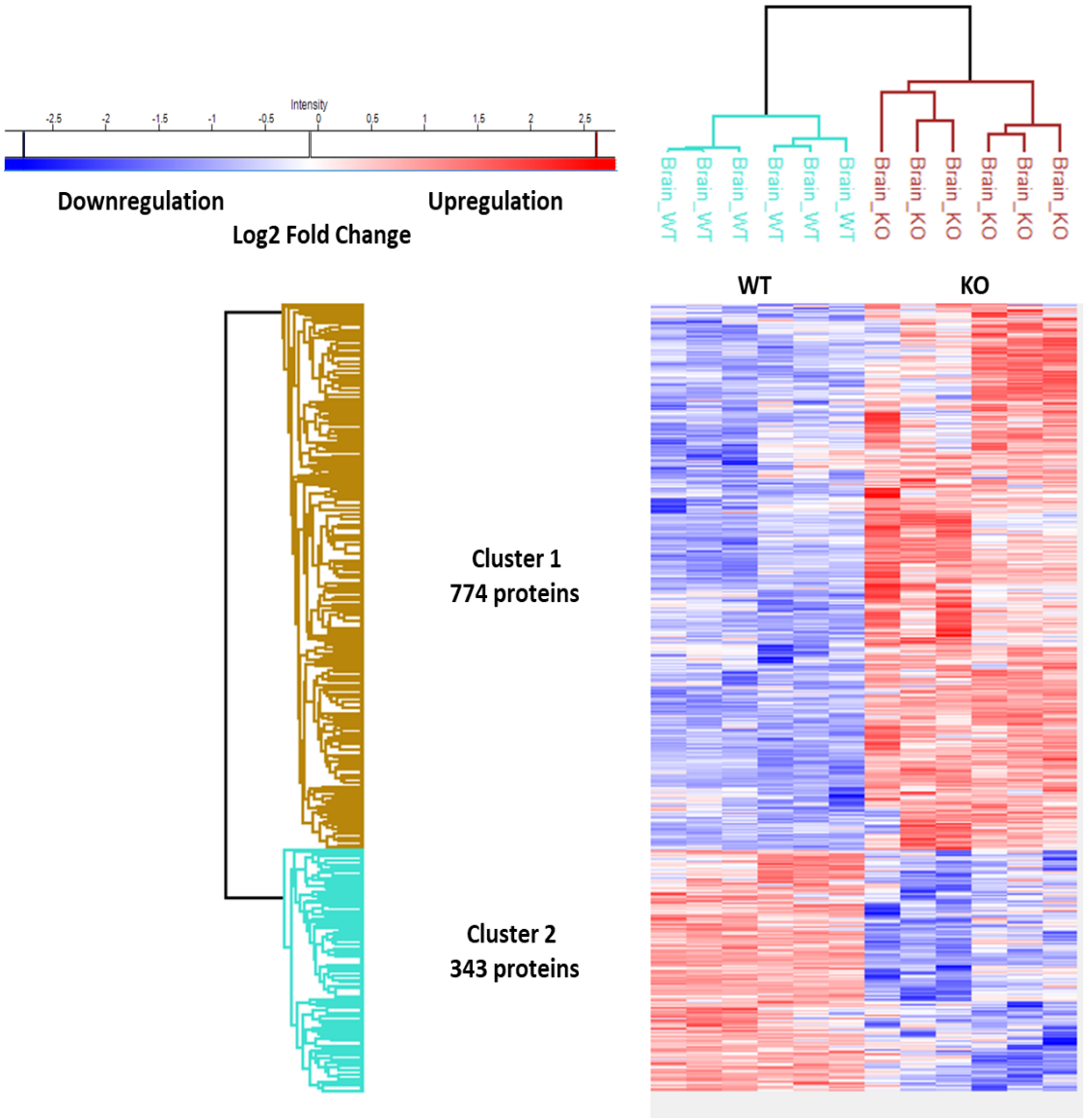

Figure 24: Heat map showing the differentially expressed proteins between WT (left) and DUSP8-KO (right) mouse brain samples. Two biological replicates were used for each condition with three technical replicates each. Potential contaminants, "reverse" and "only identified by site" hits were filtered out. The remaining intensities were log2 transformed, grouped and had their NaN (Not a Number) values replaced by low values based on normal distribution values. A two-sample Student's t-test was carried out and statistically significant intensities were normalized by z-scoring and clustered hierarchically. Two clusters with differential expression patterns were generated, one with 774 proteins (brown) and one with 343 proteins (light blue). The first cluster is associated with a general upregulation (red) in expression in KO samples, while the latter correlates to a reverse pattern (downregulation = blue) regarding the same samples.

KEGG pathways (p-value < 10^{-3})	Enrichment Factor	Gene number
Parkinson's Disease	**2.4**	**34**
Huntington's Disease	**2.2**	**35**
Oxidative phosphorylation	**2.1**	**34**
Alzheimer's Disease	**2**	**37**

Table 2: Enrichment Analysis of the two clusters showing the 4 most enriched KEGG pathways. Cluster data were exported from the heat map and matched against the data generated between the imputation step and the two-sample Student's t-test step. Fisher's Exact Test for enrichment analysis was conducted with 5% FDR. All 4 pathways were associated with more than 30 genes with statistically significant differences in their expression levels. Enrichment factors highlighted with green correspond to values higher than 1 denoting upregulation.

The four enriched KEGG pathways were examined further by matching the imputed intensities of the statistically significant proteins of each enriched pathway with the intensities of the same proteins in their non-imputed form. Imputing an intensity value, which was originally a "missing value" close to zero ("NaN") means that this value has been replaced by a random low value, in this case from the normal distribution. So, the volcano plots and heat maps show the differences between the imputed values and in order to identify proteins with theoretically infinite differences in their levels between the two conditions, we need to check their pre-imputation intensities. Two proteins associated with all four KEGG pathways were expressed in comparatively much higher levels in the brain regions of WT mice (Figure 25). These proteins were NADH dehydrogenase [ubiquinone] 1 alpha subcomplex subunit 3 (*Ndufa3*) and succinate

dehydrogenase cytochrome b560 subunit (*Sdhc*) of the mitochondrial electron transport chain.

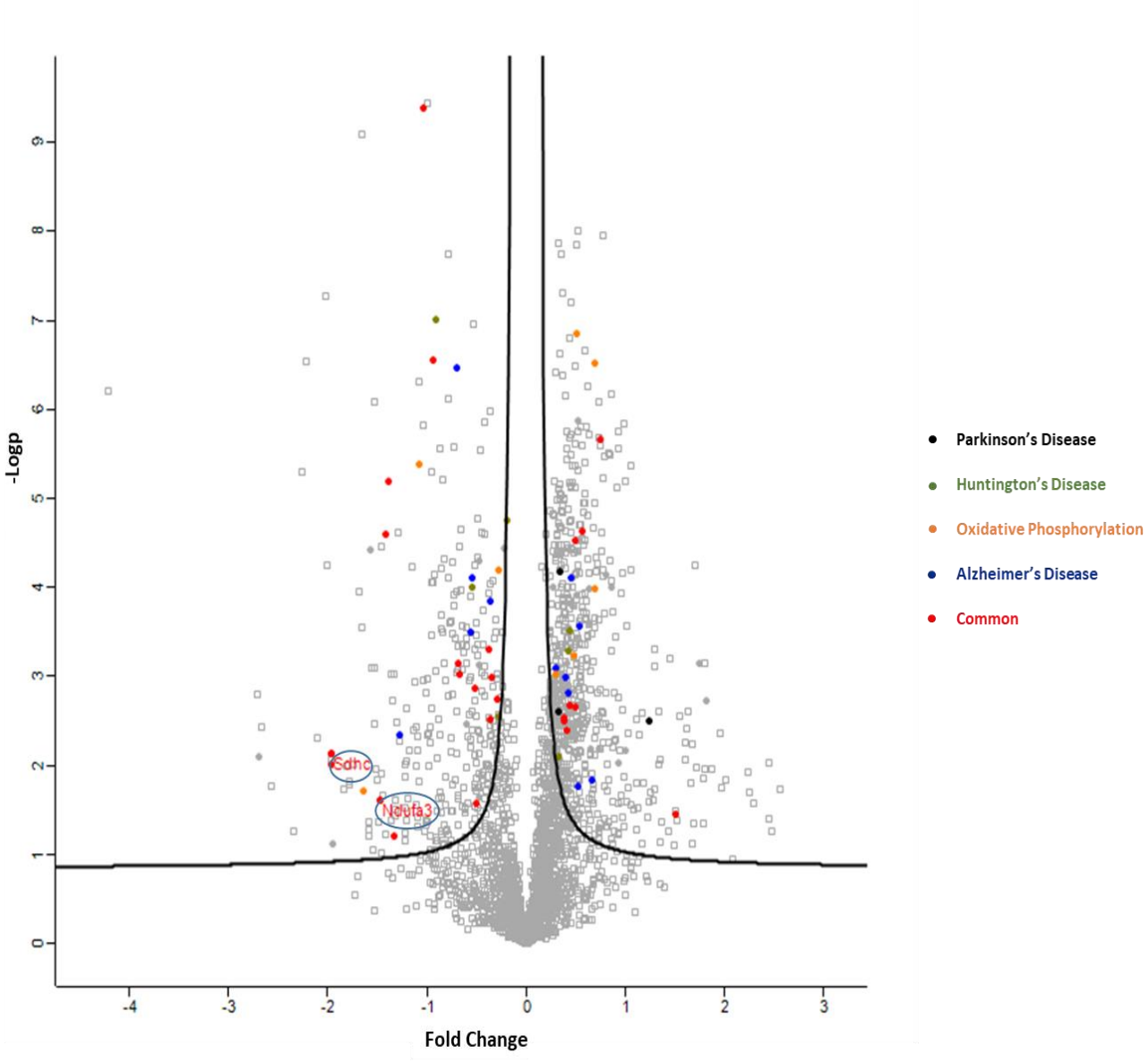

Figure 25: Volcano plot for statistically significant proteins associated with Parkinson's (black), Huntington's (green), Alzheimer's disease (blue) and oxidative phosphorylation (orange) in the brain tissues of WT and DUSP8-KO mice. Proteins involved in all four KEGG pathways are marked as red. The x-axis represents the log2 fold change of each protein's levels between the WT and KO samples, while the y-axis represents the negative log10 p-value for each protein. The right-hand side of the plot represents the upregulated, while the left-hand represents the downregulated genes expressed in the DUSP8-KO brain tissue samples. The two circled gene names correspond to the proteins NADH dehydrogenase [ubiquinone] 1 alpha subcomplex subunit 3 (Ndufa3) and succinate dehydrogenase cytochrome b560 subunit (Sdhc) of the mitochondrial electron transport chain.

All significant proteins known to be involved in the regulation of the MAPKKK signaling cascade can be seen in the volcano plot in Figure 26. The gene *Braf* expresses the serine/threonine-protein kinase B-raf, which is a MAPKKK involved in the RAF-ERK pathway. This protein was also present in much higher levels in the brain region of DUSP8-KO mice.

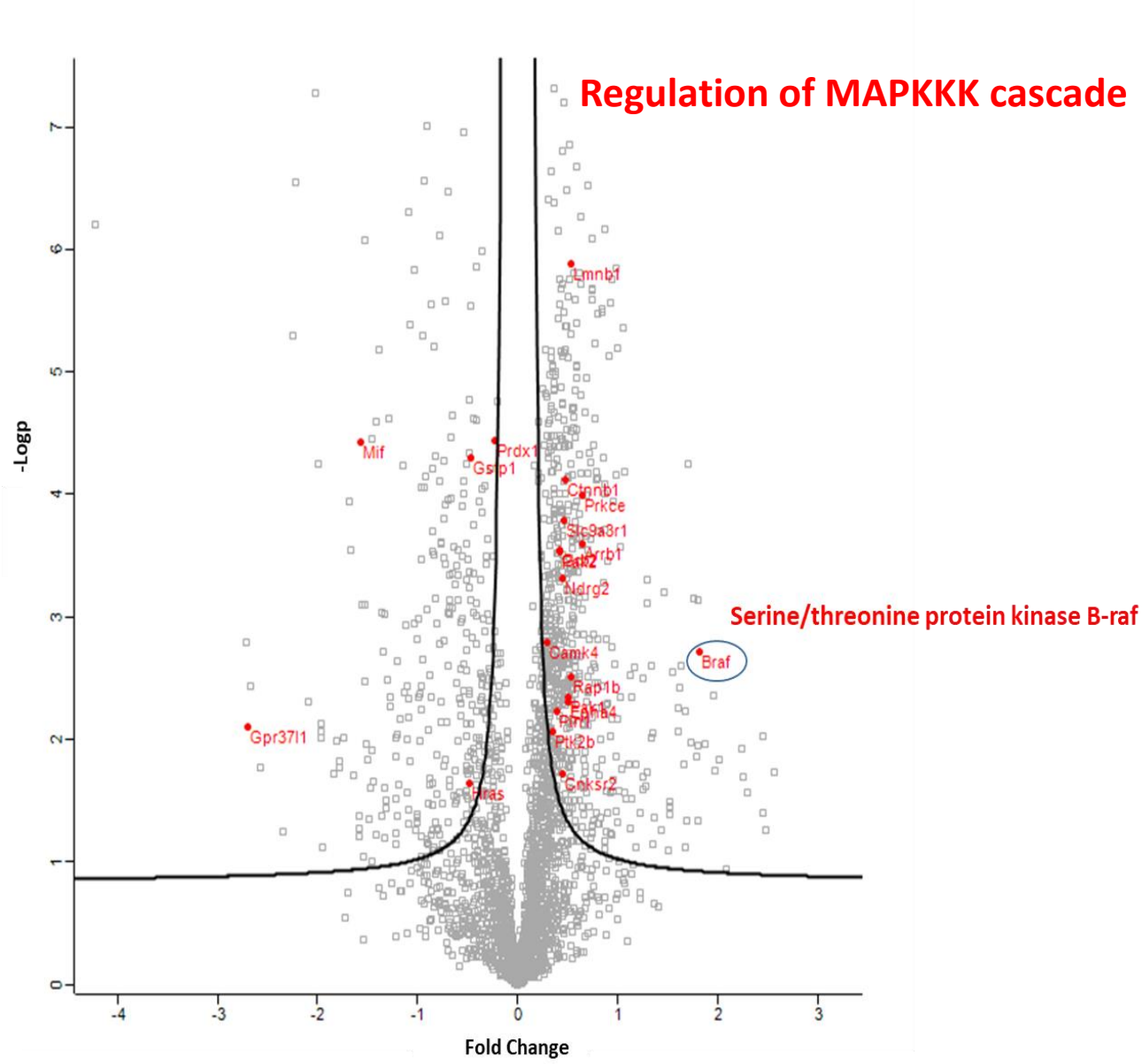

Figure 26: Volcano plot where statistically significant proteins associated with the regulation of MAPKKK cascade in the brain tissues of WT and DUSP8-KO mice are labelled in red with their corresponding gene names. The x-axis represents the log2 difference of each protein's levels between the WT and KO samples, while the y-axis represents the negative log10 p-value for each protein. The right-hand side of the plot represents the upregulated, while the left-hand represents the downregulated genes expressed in the DUSP8-KO brain tissue samples. The circled gene name corresponds to the serine/threonine protein kinase B-RAF

4. Discussion

Identification of differences in the global protein phosphorylation and protein expression due to DUSP8 deletion in mice was the main aim of this study. Therefore, an initial optimization of a phosphoproteomics workflow in HEK293T cells was a necessary procedure. 60 and 90 minutes of arsenite treatment in HEK293T cells showed higher levels of both pJNK and p-DUSP8. This finding further supports that p-DUSP8 is unable to inhibit JNK activation. Except for the pJNK levels, a wider effect of arsenite on phosphorylation was also observed. Both pSer and pTyr levels were higher in vector-only compared to DUSP8-transfected HEK293T cells. Also, comparing the time point 0 of the vector-only transfected cells with all other arsenite time points shows the significant difference between basal and induced phosphorylation levels caused by arsenite and validates it as an effective agent for stimulating a great variety of phosphorylation events. In time point 0, however, where the effect of arsenite has not taken place yet, pSer and pTyr levels were higher in DUSP8-transfected cells. A greater basal phosphorylation in cells where DUSP8 is overexpressed in contrast to a lower basal phosphorylation in cells where only the endogenous DUSP8 is present, is an interesting finding that needs to be further explored. Regarding serum starvation, western blotting experiments led to the production of unpredictable effects in a timewise manner. Its high sensitivity regarding its temporal effects ultimately did not provide a robust answer in terms of optimizing the cell culture conditions for the phosphoproteomics workflow.

From the examination of sample preparation methods based on their protein and peptide yield in the phosphoproteome analysis of HEK293T cells, FASP was found to be superior to the other two. Even though SP3 wasn't able to produce satisfying results in this study, it is still being used in other lab projects, generating more and more robust results and is steadily reaching a point of optimization.

The identified parameters of the optimized workflow were implemented in a phosphoproteome analysis of oxidative stress-induced MEFs obtained from a DUSP8-KO mouse and a WT littermate. Increased phosphorylation in a large number of proteins was observed in arsenite-treated MEFs from DUSP8-KO mice. This could be

due to the fact that some of these proteins are potential direct targets of the phosphatase and/or its deficiency caused the indirect phosphorylation of other proteins. Western blots of both pJNK and p-p38 levels were also examined in these MEFs (data not shown). Even though there were no significant differences observed among the two conditions, repeating the experiments is necessary in order to validate these results.

Regarding the phosphorylated residue percentages, serine and threonine had the most dominant presence, especially serine. This is a rational finding, since serine and threonine are the most commonly phosphorylated residues. Phosphotyrosine, on the other hand, is not easily detected due to its transient nature, which is the reason behind its generally lower phosphorylation stoichiometry and abundance in many studies[144], including this one.

The ERK1/2 pathway in MEFs, as well as in other cell types, is generally modulated by interacting with scaffolds, signaling effectors and transcriptional regulators[145]. The increased phosphorylation of some of these substrates by ERK2 in DUSP8-KO MEFs suggests a possible regulation of ERK2 by DUSP8. A similar concluding suggestion has been made from *in vivo* experiments in DUSP8-KO mice and transgenic mice with overexpressed DUSP8 specifically in cardiomyocytes[101]. So, the regulation of the ERK1/2 pathway by DUSP8 could possibly not be limited in a specific cell type.

Phosphopeptide enrichment in HEK293T lysates was carried out using a kit containing TiO_2 magnetic beads. However, the specific kit did not perform as expected and phosphopeptide enrichment for MEF lysates was conducted with TiO_2 bulk beads, which generally show a higher affinity for phosphopeptides. This could also be the main reason why enrichment in HEK293T lysates yielded poor results after MS analysis.

High DUSP8 transcript levels in brain and relatively lower in kidney mouse tissues have been detected in previous experiments of our lab (data not shown). Choosing these two types of tissues for a whole proteome analysis in DUSP8-KO mice was based on the results given by these experiments. pJNK in mouse kidneys of both WT and DUSP8-KO mice was not detected in our experiments, possibly due to low basal JNK isoform levels. Thus, JNK activation was not evaluated further in mouse kidneys. However, brain immunoblotting provided very interesting results for pJNK levels, which were elevated in DUSP8-KO mice compared to their WT littermates. It is known that DUSP8 is mostly overexpressed in the brain region, one of the few regions where

JNK3 is expressed along with JNK1 and JNK2, and its activity in the brain has higher impact compared to other tissues. So, brain DUSP8 ablation would cause a more significant increase in the activated forms of its target MAPKs and this hypothesis is supported by these findings.

Significant downregulation of protein members of the mitochondrial electron transport chain were detected in the brain region of DUSP8-KO mice. These proteins are involved in oxidative phosphorylation, so defects in their complexes cause the production of ROS, which are known to further activate the JNK pathway[146]. This could also explain the significantly higher levels of pJNK in the brain of DUSP8-KO mice. The same proteins, among others, have been shown to be downregulated in cholinergic neurons of Alzheimer's mouse models[147]. JNK pathway is also known to regulate the activation of mitochondrial-dependent apoptosis, which has been detected in many cases of neurodegeneration[148]. So, it is suggested that over activation of the JNK pathway due to DUSP8 deficiency and ROS activity potentially leads to mitochondrial apoptosis and neurodegeneration.

Except for the JNK pathway, ROS may also activate the ERK1/2 pathway as has been indicated in previous studies of neurodegeneration in both transgenic animals[149] and cell culture systems[150]. One of the MAPKKKs of this pathway is B-Raf, which was detected in comparatively much higher levels in DUSP8-KO mouse brains. As suggested by these results, ERK1/2-driven response to oxidative stress is possibly mediated mainly by the activity of B-Raf in the brain region of DUSP8-KO mice.

Western blotting experiments are needed in order to verify the presence or absence of the proteins detected only in DUSP8-KO mouse brains, like B-RAF. The biological replicates used in these studies were less than three. That makes the statistical analysis less reliable, so repeating the experiments with a higher number of replicates is one of the future plans. The following step will be the employment of targeted proteomics approaches for specific proteins of biological interest that will be detected. Whole proteome and phosphoproteome studies of tissues from DUSP8-KO and WT mice injected with arsenite is another important work that needs to be conducted in order to gain an *in vivo* perspective on the role of DUSP8 in oxidative stress response regulation.

Proteomics studies on cell signaling pathways are known to produce variable results among different labs, even when studying the effects of a specific protein. Due to the nature of these studies, it is important to generate standardized operating procedures (SOPs) for all methodologies involved and ensure their reproducibility regardless of the resource availabilities of each lab. Even though this is a very challenging task, succeeding on its implementation is a critical step towards surpassing all boundaries that decelerate the progression of proteomics in basic research.

References

1. Cooper JA, Bowen-Pope DF, Raines E, Ross R, Hunter T. Similar effects of platelet-derived growth factor and epidermal growth factor on the phosphorylation of tyrosine in cellular proteins. *Cell*. 1982;31(1):263-273. doi:10.1016/0092-8674(82)90426-3.

2. Cooper J a, Hunter T. Identification and characterization of cellular targets for tyrosine protein kinases. *J Biol Chem*. 1983;258(2):1108-1115. http://www.ncbi.nlm.nih.gov/pubmed/6571834.

3. Cooper JA. Mitogenic Stimuli and at Meiosis. 1989;9(7):3143-3147.

4. Cooper J a, Hunter T. Changes in protein phosphorylation in Rous sarcoma virus-transformed chicken embryo cells. *Mol Cell Biol*. 1981;1(2):165-178. http://www.pubmedcentral.nih.gov/articlerender.fcgi?artid=369656&tool=pmcentrez&rendertype=abstract.

5. Kazlauskas a, Cooper J a. Protein kinase C mediates platelet-derived growth factor-induced tyrosine phosphorylation of p42. *J Cell Biol*. 1988;106(4):1395-1402. doi:10.1083/jcb.106.4.1395.

6. Anderson NG, Maller JL, Tonks NK, Sturgill TW. Requirement for integration of signals from two distinct phosphorylation pathways for activation of MAP kinase. *Nature*. 1990;343(6259):651-653. doi:10.1038/343651a0.

7. Ray LB, Sturgill TW. Insulin-stimulated microtubule-associated protein kinase is phosphorylated on tyrosine and threonine in vivo. *Proc Natl Acad Sci U S A*. 1988;85(11):3753-3757. doi:10.1073/pnas.85.11.3753.

8. Boulton TG, Yancopoulos GD, Gregory JS, et al. An insulin-stiumlated protein kinase similar to yeast kinases involved in cell cycle control. *Science (80-)*. 1990;249(1988):64-67.

9. Boulton TG, Nye SH, Robbins DJ, et al. ERKs: A family of protein-serine/threonine kinases that are activated and tyrosine phosphorylated in response to insulin and NGF. *Cell*. 1991;65(4):663-675. doi:10.1016/0092-8674(91)90098-J.

10. Crews CM, Erikson RL. Crews 1993 Rev. 1993;74:215-217.

11. Roux PP, Blenis J. ERK and p38 MAPK-Activated Protein Kinases : a Family of Protein Kinases with Diverse Biological Functions ERK and p38 MAPK-Activated Protein Kinases : a Family of Protein Kinases with Diverse Biological Functions. *Microbiol Mol Biol Rev*. 2004;68(2):320-344. doi:10.1128/MMBR.68.2.320.

12. Bogoyevitch MA, Court NW. Counting on mitogen-activated protein kinases - ERKs 3, 4, 5, 6, 7 and 8. *Cell Signal*. 2004;16(12):1345-1354. doi:10.1016/j.cellsig.2004.05.004.

13. Johnson GL, Dohlman HG, Graves LM. MAPK kinase kinases (MKKKs) as a target class for small-molecule inhibition to modulate signaling networks and gene expression. *Curr Opin Chem Biol*. 2005;9(3):325-331. doi:10.1016/j.cbpa.2005.04.004.

14. Krens SFG, Spaink HP, Snaar-Jagalska BE. Functions of the MAPK family in vertebrate-development. *FEBS Lett*. 2006;580(21):4984-4990. doi:10.1016/j.febslet.2006.08.025.

15. Zhang YL, Dong C. MAP kinases in the Immune Responses. *Cell Mol Immunol*. 2005;2(1):20-27.

16. Wada T, Penninger JM. Mitogen-activated protein kinases in apoptosis regulation. *Oncogene*. 2004;23(16 REV. ISS. 2):2838-2849. doi:10.1038/sj.onc.1207556.

17. Proliferation C, Biology R, Sciences L. REVIEW MAPK signal pathways in the regulation of cell proliferation in mammalian cells. 2002;12:9-18.

18. Dan I, Watanabe NM, Kusumi A. The Ste20 group kinases as regulators of MAP kinase cascades. *Trends Cell Biol*. 2001;11(5):220-230. doi:10.1016/S0962-8924(01)01980-8.

19. KOLCH W. Meaningful relationships: the regulation of the Ras/Raf/MEK/ERK pathway by protein interactions. *Biochem J*. 2000;351(2):289-305. doi:10.1042/bj3510289.

20. Lewis TS, Shapiro PS, Ahn NG. Signal transduction through MAP kinase cascades. *Adv Cancer Res*. 1998;74:49-139.

21. Chang L, Karin M. Mammalian MAP kinase signalling cascades. *Nature*. 2001;410(6824):37-40. doi:10.1038/35065000.

22. Widmann C, Gibson S, Jarpe MB, Johnson GL. Mitogen-Activated Protein Kinase: Conservation of a Three-Kinase Module From Yeast to Human. *Physiol Rev*. 1999;79(1):143-180. doi:10.1074/jbc.271.28.16586.

23. Johnson GL, Lapadat R, Johnson GL, Lapadat R, Lapadat R. Mitogen-Activated Protein Kinase Pathways Mediated by ERK, JNK, and p38 Protein Kinases. *Science (80-)*. 2002;298(5600):1911-1912. doi:10.1126/science.1072682.

24. Tibbles L a, Woodgett JR. The stress-activated protein kinase pathways. *Cell Mol Life Sci*. 1999;55(10):1230-1254. doi:10.1007/s000180050369.

25. Zhou G, Bao ZQ, Dixon JE. Components of a new human protein kinase signal transduction pathway. *J Biol Chem*. 1995;270(21):12665-12669. doi:10.1074/jbc.270.21.12665.

26. Nishimoto S, Nishida E. MAPK signalling: ERK5 versus ERK1/2. *EMBO Rep*. 2006;7(8):782-786. doi:10.1038/sj.embor.7400755.

27. Tusa I, Gagliardi S, Tubita A, et al. ERK5 is activated by oncogenic BRAF and promotes melanoma growth. *Oncogene*. 2018;37(19):2601-2614. doi:10.1038/s41388-018-0164-9.

28. Drew BA, Burow ME, Beckman BS. MEK5/ERK5 pathway: The first fifteen years. *Biochim Biophys Acta - Rev Cancer*. 2012;1825(1):37-48. doi:10.1016/j.bbcan.2011.10.002.

29. Clapé C, Fritz V, Henriquet C, et al. miR-143 interferes with ERK5 signaling, and abrogates prostate cancer progression in mice. *PLoS One*. 2009;4(10):1-8. doi:10.1371/journal.pone.0007542.

30. Ji RR, Gereau IV RW, Malcangio M, Strichartz GR. MAP kinase and pain. *Brain Res Rev*. 2009;60(1):135-148. doi:10.1016/j.brainresrev.2008.12.011.

31. Cui Y, Wu J, Jung S-C, et al. Anti-neuroinflammatory Activity of Nobiletin on Suppression of Microglial Activation. *Biol Pharm Bull*. 2010;33(11):1814-1821. doi:10.1248/bpb.33.1814.

32. Lorenz K, Schmitt JP, Vidal M, Lohse MJ. Cardiac hypertrophy: Targeting Raf/MEK/ERK1/2-signaling. *Int J Biochem Cell Biol*. 2009;41(12):2351-2355. doi:10.1016/j.biocel.2009.08.002.

33. Zhu C, Qi X, Chen Y, Sun B, Dai Y, Gu Y. PI3K/Akt and MAPK/ERK1/2 signaling pathways are involved in IGF-1-induced VEGF-C upregulation in breast cancer. *J Cancer Res Clin Oncol*. 2011;137(11):1587-1594. doi:10.1007/s00432-011-1049-2.

34. Sun J, Nan G. The extracellular signal-regulated kinase 1/2 pathway in neurological diseases: A potential therapeutic target (Review). *Int J Mol Med*. 2017;39(6):1338-1346. doi:10.3892/ijmm.2017.2962.

35. Yao Z, Seger R. The ERK signaling cascade-views from different subcellular compartments. *BioFactors*. 2009;35(5):407-416. doi:10.1002/biof.52.

36. Wu Z, Ou L, Wang C, et al. Icaritin induces MC3T3-E1 subclone14 cell differentiation through estrogen receptor-mediated ERK1/2 and p38 signaling activation. *Biomed Pharmacother*. 2017;94:1-9. doi:10.1016/j.biopha.2017.07.071.

37. Senger K, Pham VC, Varfolomeev E, et al. The kinase TPL2 activates ERK and p38 signaling to promote neutrophilic inflammation. *Sci Signal*. 2017;10(475). doi:10.1126/scisignal.aah4273.

38. Zou X, Blank M. Targeting p38 MAP kinase signaling in cancer through post-translational modifications. *Cancer Lett*. 2017;384:19-26. doi:10.1016/j.canlet.2016.10.008.

39. Ono K, Han J. The p38 signal transduction pathway: activation and function. *Cell Signal*. 2000;12:1-13. doi:S0898-6568(99)00071-6 [pii].

40. New L, Han J. The p38 MAP kinase pathway and its biological function. *Trends Cardiovasc Med*. 1998;8(5):220-228. doi:10.1016/S1050-1738(98)00012-7.

41. Rouse J, Cohen P, Trigon S, et al. A novel kinase cascade triggered by stress and heat shock that stimulates MAPKAP kinase-2 and phosphorylation of the small heat shock proteins. *Cell*. 1994;78(6):1027-1037. doi:10.1016/0092-8674(94)90277-1.

42. Moriguchi T, Kuroyanagi N, Yamaguchi K. A novel kinase cascade mediated by mitogen activated protein kinase 6 and MKK3. *J Biol Chem*. 1996;271(23):13675-13679. doi:10.1074/jbc.271.23.13675.

43. Hirai S, Katoh M, Kyriakis JM, et al. MST / MLK2 , a Member of the Mixed Lineage Kinase Family , Directly Phosphorylates and Activates SEK1 , an MST / MLK2 , a Member of the Mixed Lineage Kinase Family , Directly Phosphorylates and Activates SEK1 , an Activator of c-Jun N-terminal Kinase / St. *Enzymology*. 1997;272(24):15167-15173. doi:10.1074/jbc.272.24.15167.

44. Cuenda a, Dorow DS. Differential activation of stress-activated protein kinase kinases SKK4/MKK7 and SKK1/MKK4 by the mixed-lineage kinase-2 and mitogen-activated

protein kinase kinase (MKK) kinase-1. *Biochem J*. 1998;333 (Pt 1:11-15. doi:10.1042/bj3330011.

45. Zarubin T, Han J. Activation and signaling of the p38 MAP kinase pathway. *Cell Res*. 2005;15(1):11-18. doi:10.1038/sj.cr.7290257.

46. Han J, Ulevitch J. A MAP Kinase Targeted by Endotoxin and Hyperosmolarity in Mammalian Cells. 1994;2:1-4.

47. Han J, Lee JD, Tobias PS, Ulevitch RJ. Endotoxin induces rapid protein tyrosine phosphorylation in 70Z/3 cells expressing CD14. *J Biol Chem*. 1993;268(33):25009-25014.

48. Jiang Y, Chen C, Li Z. Characterization of the structure and function of a new mitogen-activated protein kinase (p38[beta]). *J Biol Chem*. 1996;271(30):17920-17926. http://dx.doi.org/10.1074/JBC.271.30.17920.

49. Li Z, Jiang Y, Ulevitch RJ, Han J. The primary structure of p38gamma: a new member of p38 group of MAP kinases. *Biochem Biophys Res Commun*. 1996;228:334-340. doi:10.1006/bbrc.1996.1662.

50. Lechner C, Zahalka MA, Giot JF, Møller NP, Ullrich A. ERK6, a mitogen-activated protein kinase involved in C2C12 myoblast differentiation. *Proc Natl Acad Sci U S A*. 1996;93(9):4355-4359. doi:10.1073/pnas.93.9.4355.

51. Kumar S, McDonnell PC, Gum RJ, Hand AT, Lee JC, Young PR. Novel homologues of CSBP/p38 MAP kinase: Activation, substrate specificity and sensitivity to inhibition by pyridinyl imidazoles. *Biochem Biophys Res Commun*. 1997;235(3):533-538. doi:10.1006/bbrc.1997.6849.

52. Jiang Y, Gram H, Zhao M, et al. CELL BIOLOGY AND METABOLISM : Characterization of the Structure and Function of the Fourth Member of p38 Characterization of the Structure and Function of the Fourth Member of p38 Group Mitogen-activated Protein Kinases , p38 □ *. 1997;272(48):30122-30128. doi:10.1074/jbc.272.48.30122.

53. Wang Z, Harkins PC, Ulevitch RJ, Han J, Cobb MH, Goldsmith EJ. The structure of mitogen-activated protein kinase p38 at 2.1-A resolution. *Proc Natl Acad Sci U S A*. 1997;94(6):2327-2332. doi:10.1073/pnas.94.6.2327.

54. Del Arco PG, Martínez-Martínez S, Maldonado JL, Ortega-Pérez I, Redondo JM. A role for the p38 MAP kinase pathway in the nuclear shuttling of NFATp. *J Biol Chem*.

2000;275(18):13872-13878. doi:10.1074/jbc.275.18.13872.

55. Huang C, Ma WY, Maxiner A, Sun Y, Dong Z. p38 kinase mediates UV-induced phosphorylation of p53 protein at serine 389. *J Biol Chem*. 1999;274(18):12229-12235. doi:10.1074/jbc.274.18.12229.

56. Hazzalin CA, Cano E, Cuenda A, Barratt MJ, Cohen P, Mahadevan LC. p38/RK is essential for stress-induced nuclear responses: JNK/SAPKs and c-Jun/ATF-2 phosphorylation are insufficient. *Curr Biol*. 1996;6(8):1028-1031. doi:10.1016/S0960-9822(02)00649-8.

57. Tan Y, Rouse J, Zhang A, Cariati S, Cohen P, Comb MJ. FGF and stress regulate CREB and ATF-1 via a pathway involving p38 MAP kinase and MAPKAP kinase-2. *EMBO J*. 1996;15(17):4629-4642. doi:10.1002/j.1460-2075.1996.tb00840.x.

58. Reynolds CH, Nebreda a R, Gibb GM, Utton M a, Anderton BH. Reactivating kinase/p38 phosphorylates tau protein in vitro. *J Neurochem*. 1997;69:191-198.

59. McLaughlin MM, Kumar S, McDonnell PC, et al. Identification of mitogen-activated protein (MAP) kinase-activated protein kinase-3, a novel substrate of GSBP p38 MAP kinase. *JBiolChem*. 1996;271(14):8488-8492.

60. Gallo KA, Johnson GL. Mixed-lineage kinase control of JNK and p38 MAPK pathways. *Nat Rev Mol Cell Biol*. 2002;3(9):663-672. doi:10.1038/nrm906.

61. Wagner EF, Nebreda ÁR. Signal integration by JNK and p38 MAPK pathways in cancer development. *Nat Rev Cancer*. 2009;9(8):537-549. doi:10.1038/nrc2694.

62. Johnson GL, Nakamura K. The c-jun kinase/stress-activated pathway: Regulation, function and role in human disease. *Biochim Biophys Acta - Mol Cell Res*. 2007;1773(8):1341-1348. doi:10.1016/j.bbamcr.2006.12.009.

63. Murphy LO, Blenis J. MAPK signal specificity: the right place at the right time. *Trends Biochem Sci*. 2006;31(5):268-275. doi:10.1016/j.tibs.2006.03.009.

64. Dérijard B, Hibi M, Wu IH, et al. JNK1: A protein kinase stimulated by UV light and Ha-Ras that binds and phosphorylates the c-Jun activation domain. *Cell*. 1994;76(6):1025-1037. doi:10.1016/0092-8674(94)90380-8.

65. Pulverer BJ, Kyriakis JM, Avruch J, Nikolakaki E, Woodgett JR. Phosphorylation of c-jun mediated by MAP kinases. *Nature*. 1991;353(6345):670-674.

doi:10.1038/353670a0.

66. Smeal T, Binetruy B, Mercola D, et al. Oncoprotein-Mediated Signalling Cascade Stimulates c-Jun Activity by Phosphorylation of Serines 63 and 73. *Mol Cell Biol*. 1992;12(8):3507-3513. doi:10.1128/MCB.12.8.3507.Updated.

67. Yang DD, Kuan CY, Whitmarsh AJ, et al. Absence of excitotoxicity-induced apoptosis in the hippocampus of mice lacking the Jnk3 gene. *Nature*. 1997;389(6653):865-870. doi:10.1038/39899.

68. Wang Y. Mitogen-activated protein kinases in heart development and diseases. *Circulation*. 2007;116(12):1413-1423. doi:10.1161/CIRCULATIONAHA.106.679589.

69. Kuan C-Y, Yang DD, Roy DRS, Davis RJ, Rakic P, Flavell R a. The Jnk1 and Jnk2 Protein Kinases Are Required for Regional\rSpecific Apoptosis during Early Brain Development. *Neuron*. 1999;22:667-676. doi:10.1016/S0896-6273(00)80727-8.

70. Sabapathy K, Jochum W, Hochedlinger K, Chang L, Karin M, Wagner EF. Defective neural tube morphogenesis and altered apoptosis in the absence of both JNK1 and JNK2. *Mech Dev*. 1999;89(1-2):115-124. doi:10.1016/S0925-4773(99)00213-0.

71. Chang L, Jones Y, Ellisman MH, Goldstein LSB, Karin M. JNK1 is required for maintenance of neuronal microtubules and controls phosphorylation of microtubule-associated proteins. *Dev Cell*. 2003;4(4):521-533. doi:10.1016/S1534-5807(03)00094-7.

72. Kallunki T, Su B, Tsigelny I, et al. JNK2 contains a specificity-determining region responsible for efficient c-Jun binding and phosphorylation. *Genes Dev*. 1994;8(24):2996-3007. doi:10.1101/gad.8.24.2996.

73. Gupta S, Barrett T, Whitmarsh a J, et al. Selective interaction of JNK protein kinase isoforms with transcription factors. *EMBO J*. 1996;15(11):2760-2770. doi:10.1002/j.1460-2075.1996.tb00636.x.

74. Kato T, Noma H, Kitagawa M, Takahashi T, Oshitani N, Kitagawa S. Distinct role of c-Jun N-terminal kinase isoforms in human neutrophil apoptosis regulated by tumor necrosis factor-alpha and granulocyte-macrophage colony-stimulating factor. *J Interferon Cytokine Res*. 2008;28(4):235-243. doi:10.1089/jir.2007.0075.

75. Brecht S, Kirchhof R, Chromik A, et al. Specific pathophysiological functions of JNK isoforms in the brain. *Eur J Neurosci*. 2005;21(2):363-377. doi:10.1111/j.1460-

9568.2005.03857.x.

76. Dreskin SC, Thomas GW, Dale SN, Heasley LE. Isoforms of Jun Kinase Are Differentially Expressed and Activated in Human Monocyte/Macrophage (THP-1) Cells. *J Immunol*. 2001;166(9):5646-5653. doi:10.4049/jimmunol.166.9.5646.

77. Ichijo H. From receptors to stress-activated MAP kinases. *Oncogene*. 1999;18(45):6087-6093. doi:10.1038/sj.onc.1203129.

78. Eriksson M, Taskinen M, Leppä S. Mitogen Activated Protein Kinase-Dependent Activation of c-Jun and c-Fos is required for Neuronal differentiation but not for Growth and Stress Reposne in PC12 cells. *J Cell Physiol*. 2006;207(1):12-22. doi:10.1002/JCP.

79. Leppä S, Bohmann D. Diverse functions of JNK signaling and c-Jun in stress response and apoptosis. *Oncogene*. 1999;18(45):6158-6162. doi:10.1038/sj.onc.1203173.

80. Kyriakis JM. Signaling by the germinal center kinase family of protein kinases. *JBiol Chem*. 1999;274(9):5259-5262. http://www.ncbi.nlm.nih.gov/pubmed/0010026130.

81. Bogoyevitch MA, Ngoei KRW, Zhao TT, Yeap YYC, Ng DCH. c-Jun N-terminal kinase (JNK) signaling: Recent advances and challenges. *Biochim Biophys Acta - Proteins Proteomics*. 2010;1804(3):463-475. doi:10.1016/j.bbapap.2009.11.002.

82. Karin M, Gallagher E. From JNK to pay dirt: Jun kinases, their biochemistry, physiology and clinical importance. *IUBMB Life*. 2005;57(4-5):283-295. doi:10.1080/15216540500097111.

83. Morrison DK, Davis RJ. Regulation of MAP Kinase Signaling Modules by Scaffold Proteins in Mammals. *Annu Rev Cell Dev Biol*. 2003;19(1):91-118. doi:10.1146/annurev.cellbio.19.111401.091942.

84. Han J, Cox DG, Colditz G a, Hunter DJ. The p53 codon 72 polymorphism, sunburns, and risk of skin cancer in US Caucasian women. *Mol Carcinog*. 2006;45(9):694-700. doi:10.1002/mc.

85. Mustelin T. A brief introduction to the protein phosphatase families. *Methods Mol Biol*. 2007;365:9-22. doi:10.1385/1-59745-267-X:9.

86. Dickinson RJ, Keyse SM. Diverse physiological functions for dual-specificity MAP kinase phosphatases. *J Cell Sci*. 2006;119(22):4607-4615. doi:10.1242/jcs.03266.

87. Denu JM, Dixon JE. A catalytic mechanism for the dual-specific phosphatases. *Proc Natl Acad Sci U S A*. 1995;92(13):5910-5914. doi:10.1073/pnas.92.13.5910.

88. Patterson KI, Brummer T, O'brien PM, Daly RJ. Dual-specificity phosphatases: critical regulators with diverse cellular targets. *Biochem J*. 2009;418(3):475-489. doi:10.1042/BJ20082234.

89. Huang CY, Tan TH. DUSPs, to MAP kinases and beyond. *Cell Biosci*. 2012;2(1):1-10. doi:10.1186/2045-3701-2-24.

90. Nichols A, Camps M, Gillieron C, et al. Substrate recognition domains within extracellular signal-regulated kinase mediate binding and catalytic activation of mitogen-activated protein kinase phosphatase-3. *J Biol Chem*. 2000;275(32):24613-24621. doi:10.1074/jbc.M001515200.

91. Tanoue T, Adachi M, Moriguchi T, Nishida E. A conserved docking motif in MAP kinases common to substrates, activators and regulators. *Nat Cell Biol*. 2000;2(2):110-116. doi:10.1038/35000065.

92. Keyse SM, Ginsburg M. Amino acid sequence similarity between CL100, a dual-specificity MAP kinase phosphatase and cdc25. *Trends Biochem Sci*. 1993;18(10):377. http://www.ncbi.nlm.nih.gov/pubmed/8256285.

93. Bordo D, Bork P. The rhodanese/Cdc25 phosphatase superfamily. 2002;3(8):741-746.

94. Owens DM, Keyse SM. Differential regulation of MAP kinase signalling by dual-specificity protein phosphatases. *Oncogene*. 2007;26(22):3203-3213. doi:10.1038/sj.onc.1210412.

95. Caunt CJ, Keyse SM. Dual-specificity MAP kinase phosphatases (MKPs): Shaping the outcome of MAP kinase signalling. *FEBS J*. 2013;280(2):489-504. doi:10.1111/j.1742-4658.2012.08716.x.

96. Muda M, Theodosiou A, Rodrigues N, et al. The dual specificity phosphatases M3/6 and MKP-3 are Highly Selective for Inactivation of Distinct Mitogen- activated Protein Kinases *. 1996:27205-27208.

97. Johnson TR, Biggs JR, Winbourn SE, Kraft AS. Regulation of dual-specificity phosphatases M3/6 and hVH5 by phorbol esters. Analysis of a delta-like domain. *J Biol Chem*. 2000;275(41):31755-31762. doi:10.1074/jbc.M004182200.

98. Okami N, Narasimhan P, Yoshioka H, et al. Prevention of JNK phosphorylation as a mechanism for rosiglitazone in neuroprotection after transient cerebral ischemia: Activation of dual specificity phosphatase. *J Cereb Blood Flow Metab*. 2013;33(1):106-114. doi:10.1038/jcbfm.2012.138.

99. Rechsteiner M, Rogers SW. PEST sequences and regulation by proteolysis. *Trends Biochem Sci*. 1996;21(7):267-271. doi:10.1016/S0968-0004(96)10031-1.

100. Theodosiou AM, Rodrigues NR, Nesbit MA, et al. A member of the MAP kinase phosphatase gene family in mouse containing a complex trinucleotide repeat in the coding region. *Hum Mol Genet*. 1996;5(5):675-684. doi:10.1093/hmg/5.5.675.

101. Liu R, Van Berlo JH, York AJ, Vagnozzi RJ, Maillet M, Molkentin JD. DUSP8 Regulates Cardiac Ventricular Remodeling by Altering ERK1/2 Signaling. *Circ Res*. 2016;119(2):249-260. doi:10.1161/CIRCRESAHA.115.308238.

102. Oehrl W, Cotsiki M, Panayotou G. Differential regulation of M3/6 (DUSP8) signaling complexes in response to arsenite-induced oxidative stress. *Cell Signal*. 2013;25(2):429-438. doi:10.1016/j.cellsig.2012.11.010.

103. Cotsiki M, Oehrl W, Samiotaki M, Theodosiou A, Panayotou G. Phosphorylation of the m3/6 dual-specificity phosphatase enhances the activation of jnk by arsenite. *Cell Signal*. 2012;24(3):664-676. doi:10.1016/j.cellsig.2011.10.015.

104. Cavigelli M, Li WW, Lin A, Su B, Yoshioka K, Karin M. The tumor promoter arsenite stimulates AP-1 activity by inhibiting a JNK phosphatase. *EMBO J*. 1996;15(22):6269-6279. http://www.pubmedcentral.nih.gov/articlerender.fcgi?artid=452450&tool=pmcentrez&rendertype=abstract.

105. Kamata H, Honda SI, Maeda S, Chang L, Hirata H, Karin M. Reactive oxygen species promote TNFα-induced death and sustained JNK activation by inhibiting MAP kinase phosphatases. *Cell*. 2005;120(5):649-661. doi:10.1016/j.cell.2004.12.041.

106. Huang C, Ma WY, Li J, Goranson A, Dong Z. Requirement of Erk, but not JNK, for arsenite-induced cell transformation. *J Biol Chem*. 1999;274(21):14595-14601. doi:10.1074/jbc.274.21.14595.

107. Huang C, Li J, Dong Z. Advances in Brief Arsenic Induces Apoptosis through a c-Jun NH 2 -Terminal Kinase-dependent , p53-independent pathway. *Cancer Res*.

1999;59(july):3053-3058.

108. Bode AM, Dong Z. The paradox of arsenic: Molecular mechanisms of cell transformation and chemotherapeutic effects. *Crit Rev Oncol Hematol*. 2002;42(1):5-24. doi:10.1016/S1040-8428(01)00215-3.

109. Tobiume K, Matsuzawa A, Takahashi T, et al. ASK1 is required for sustained activations of JNK/p38 MAP kinases and apoptosis. *EMBO Rep*. 2001;2(3):222-228. doi:10.1093/embo-reports/kve046.

110. Austin CP, Battey JF, Bradley A, et al. The Knockout Mouse Project. *Nat Genet*. 2004;36(9):921-924. doi:10.1038/ng0904-921.

111. Ran FA, Hsu PD, Wright J, Agarwala V, Scott DA, Zhang F. Genome engineering using the CRISPR-Cas9 system. *Nat Protoc*. 2013;8(11):2281-2308. doi:10.1038/nprot.2013.143.

112. Towbin H, Staehelin T, Gordon J. Electrophoretic transfer of proteins from polyacrylamide gels to nitrocellulose sheets: procedure and some applications. *Proc Natl Acad Sci*. 1979;76(9):4350-4354. doi:10.1073/pnas.76.9.4350.

113. Aebersold R, Burlingame AL, Bradshaw RA. Western Blots *versus* Selected Reaction Monitoring Assays: Time to Turn the Tables? *Mol Cell Proteomics*. 2013;12(9):2381-2382. doi:10.1074/mcp.E113.031658.

114. Gross JH. *Mass Spectrometry*.; 2002. doi:10.1002/0471440264.pst190.

115. Lee WC, Lee KH. Applications of affinity chromatography in proteomics. *Anal Biochem*. 2004;324(1):1-10. doi:10.1016/j.ab.2003.08.031.

116. Tran JC, Zamdborg L, Ahlf DR, et al. Mapping intact protein isoforms in discovery mode using top-down proteomics. *Nature*. 2011;480(7376):254-258. doi:10.1038/nature10575.

117. Boone C, Adamec J. *Top-Down Proteomics*. Second Edi. Elsevier; 2016. doi:10.1016/B978-0-444-63688-1.00010-0.

118. Zubarev RA, Makarov A. Orbitrap Mass Spectrometry. *Anal Chem*. 2013;85(11):5288-5296. doi:10.1021/ac4001223.

119. Gillet LC, Navarro P, Tate S, et al. Targeted Data Extraction of the MS/MS Spectra Generated by Data-independent Acquisition: A New Concept for Consistent and

Accurate Proteome Analysis. *Mol Cell Proteomics*. 2012;11(6):O111.016717. doi:10.1074/mcp.O111.016717.

120. Aebersold R, Mann M. Mass-spectrometric exploration of proteome structure and function. *Nature*. 2016;537(7620):347-355. doi:10.1038/nature19949.

121. Fílla J, Honys D. Enrichment techniques employed in phosphoproteomics. *Amino Acids*. 2012;43(3):1025-1047. doi:10.1007/s00726-011-1111-z.

122. Engholm-Keller K, Larsen MR. Technologies and challenges in large-scale phosphoproteomics. *Proteomics*. 2013;13(6):910-931. doi:10.1002/pmic.201200484.

123. Hsu CC, Xue L, Arrington J V., et al. Estimating the Efficiency of Phosphopeptide Identification by Tandem Mass Spectrometry. *J Am Soc Mass Spectrom*. 2017;28(6):1127-1135. doi:10.1007/s13361-017-1603-5.

124. Sugiyama N, Masuda T, Shinoda K, Nakamura A, Tomita M, Ishihama Y. Phosphopeptide Enrichment by Aliphatic Hydroxy Acid-modified Metal Oxide Chromatography for Nano-LC-MS/MS in Proteomics Applications. *Mol Cell Proteomics*. 2007;6(6):1103-1109. doi:10.1074/mcp.T600060-MCP200.

125. Tsai CF, Hsu CC, Hung JN, et al. Sequential phosphoproteomic enrichment through complementary metal-directed immobilized metal ion affinity chromatography. *Anal Chem*. 2014;86(1):685-693. doi:10.1021/ac4031175.

126. Buydens L, Ampt K, Stingl C, Dane A. MCP Papers in Press. Published on June 7, 2010 as Manuscript M110.000877. 2010;(31):1-46.

127. Rush J, Moritz A, Lee KA, et al. Immunoaffinity profiling of tyrosine phosphorylation in cancer cells. *Nat Biotechnol*. 2005;23(1):94-101. doi:10.1038/nbt1046.

128. Winter D, Seidler J, Ziv Y, Shiloh Y, Lehmann WD. Citrate boosts the performance of phosphopeptide analysis by UPLC-ESI-MS/MS. *J Proteome Res*. 2009;8(1):418-424. doi:10.1021/pr800304n.

129. Cawley AT, Flenker U. The application of carbon isotope ratio mass spectrometry to doping control. *J Mass Spectrom*. 2008;43(7):854-864. doi:10.1002/jms.

130. Olsen J V., Mann M. Improved peptide identification in proteomics by two consecutive stages of mass spectrometric fragmentation. *Proc Natl Acad Sci*. 2004;101(37):13417-13422. doi:10.1073/pnas.0405549101.

131. Schroeder MJ, Shabanowitz J, Schwartz JC, Hunt DF, Coon JJ. A neutral loss activation method for improved phosphopeptide sequence analysis by quadrupole ion trap mass spectrometry. *Anal Chem*. 2004;76(13):3590-3598. doi:10.1021/ac0497104.

132. Iliuk AB, Arrington J V., Tao WA. Analytical challenges translating mass spectrometry-based phosphoproteomics from discovery to clinical applications. *Electrophoresis*. 2014;35(24):3430-3440. doi:10.1002/elps.201400153.

133. Kingston RE. Introduction of DNA into Mammalian Cells. *Curr Protoc Mol Biol*. 2003;64(1):1-5. doi:10.1002/0471142727.mb0900s64.

134. Muda M, Boschert U, Dickinson R, et al. MKP-3, a novel cytosolic protein-tyrosine phosphatase that examplifies a new class of mitogen-activated protein kinase phosphatase. *J Biol Chem*. 1996;271(8):4319-4326. doi:10.1074/jbc.271.8.4319.

135. Moggridge S, Sorensen PH, Morin GB, Hughes CS. Extending the Compatibility of the SP3 Paramagnetic Bead Processing Approach for Proteomics. *J Proteome Res*. 2018;17(4):1730-1740. doi:10.1021/acs.jproteome.7b00913.

136. Humphrey SJ, Azimifar SB, Mann M. High-throughput phosphoproteomics reveals in vivo insulin signaling dynamics. *Nat Biotechnol*. 2015;33(9):990-995. doi:10.1038/nbt.3327.

137. Thingholm TE, Jørgensen TJD, Jensen ON, Larsen MR. Highly selective enrichment of phosphorylated peptides using titanium dioxide. *Nat Protoc*. 2006;1(4):1929-1935. doi:10.1038/nprot.2006.185.

138. Kyono Y, Sugiyama N, Imami K, Tomita M, Ishihama Y. Successive and selective release of phosphorylated peptides captured by hydroxy acid-modified metal oxide chromatography. *J Proteome Res*. 2008;7(10):4585-4593. doi:10.1021/pr800305y.

139. Cox J, Mann M. MaxQuant enables high peptide identification rates, individualized p.p.b.-range mass accuracies and proteome-wide protein quantification. *Nat Biotechnol*. 2008;26(12):1367-1372. doi:10.1038/nbt.1511.

140. Tyanova S, Temu T, Sinitcyn P, et al. The Perseus computational platform for comprehensive analysis of (prote)omics data. *Nat Methods*. 2016;13(9):731-740. doi:10.1038/nmeth.3901.

141. Wang F. Culture of Animal Cells: a Manual of Basic Technique, Fifth Edition. *Vitr Cell Dev Biol - Anim*. 2006;42(5):169. doi:10.1290/BR090501.1.

142. Herren A, Searle B, Leib R, et al. *R F ABRF-sPRG 2017-2018 : Development and Characterization of a Stable-Isotope Labeled Phosphopeptide Standard*.; 2018.

143. Eng JK, McCormack AL, Yates JR. An approach to correlate tandem mass spectral data of peptides with amino acid sequences in a protein database. *J Am Soc Mass Spectrom*. 1994;5(11):976. doi:10.1016/1044-0305(94)80016-2.

144. Batth TS, Papetti M, Pfeiffer A, Tollenaere MAX, Francavilla C, Olsen J V. Large-Scale Phosphoproteomics Reveals Shp-2 Phosphatase-Dependent Regulators of Pdgf Receptor Signaling. *Cell Rep*. 2018;22(10):2601-2614. doi:10.1016/j.celrep.2018.02.038.

145. Voisin L, Saba-El-Leil MK, Julien C, Fremin C, Meloche S. Genetic Demonstration of a Redundant Role of Extracellular Signal-Regulated Kinase 1 (ERK1) and ERK2 Mitogen-Activated Protein Kinases in Promoting Fibroblast Proliferation. *Mol Cell Biol*. 2010;30(12):2918-2932. doi:10.1128/MCB.00131-10.

146. Son Y, Cheong Y-K, Kim N-H, Chung H-T, Kang DG, Pae H-O. Mitogen-Activated Protein Kinases and Reactive Oxygen Species: How Can ROS Activate MAPK Pathways? *J Signal Transduct*. 2011;2011:1-6. doi:10.1155/2011/792639.

147. McKeever PM, Kim TH, Hesketh AR, et al. Cholinergic neuron gene expression differences captured by translational profiling in a mouse model of Alzheimer's disease. *Neurobiol Aging*. 2017;57:104-119. doi:10.1016/j.neurobiolaging.2017.05.014.

148. Perier C, Bove J, Wu D-C, et al. Two molecular pathways initiate mitochondria-dependent dopaminergic neurodegeneration in experimental Parkinson's disease. *Proc Natl Acad Sci*. 2007;104(19):8161-8166. doi:10.1073/pnas.0609874104.

149. Noshita N, Sugawara T, Hayashi T, Lewen A, Omar G, Chan PH. Copper/Zinc Superoxide Dismutase Attenuates Neuronal Cell Death by Preventing Extracellular Signal-Regulated Kinase Activation after Transient Focal Cerebral Ischemia in Mice. *J Neurosci*. 2002;22(18):7923-7930. http://www.jneurosci.org/cgi/content/abstract/22/18/7923.

150. Zhu JH, Kulich SM, Oury TD, Chu CT. Cytoplasmic aggregates of phosphorylated extracellular signal-regulated protein kinases in lewy body diseases. *Am J Pathol*. 2002;161(6):2087-2098. doi:10.1016/S0002-9440(10)64487-2.